

FIRBACK IV. Towards the nature of the 170 μm source population

Dennefeld M.^{1*}, Lagache G.², Mei S.^{2,3}, Ciliegi P.⁴, Dole H.², Mann R.G.⁵,
Taylor E.L.⁵, Vaccari M.⁶

¹ Institut d'Astrophysique de Paris, 98bis Boulevard Arago, F-75014 Paris

² Institut d'Astrophysique Spatiale, Bât. 121, Université Paris XI, F-91405 Orsay

³ Johns Hopkins University, 3400 N. Charles Street, 21218, Baltimore, MD, USA

⁴ INAF-Osservatorio Astronomico di Bologna, via Ranzani 1, I-40127 Bologna

⁵ Institute for Astronomy, University of Edinburg, Royal Observatory, Blackford Hill, Edinburgh, EH9 3HJ United Kingdom

⁶ Astrophysics Group, Blackett Laboratory, Imperial College, Prince Consort Road, SW7 2AZ London

Received 13 August 2004; Accepted 14 march 2005

Abstract. We present a detailed study of the brighter ($> 4\sigma$ detections) sources in the 170 μm FIRBACK northern N1 ISO survey, with the help of complementary data in the optical, radio, and mid-IR domain. For 82% of them, an optical galaxy counterpart is identified, either as the unique source of the IR emission, or as part of a multiple identification. With less than 15% of AGNs, these sources are essentially local, moderate starbursters with a dominating cold dust component. They are therefore very similar to the galaxies in the IRAS Very Faint Survey or the ISO 170 μm Serendipity Survey, and represent a population of cold galaxies rather neglected up to now. Their colours do not match those of the far-IR Cosmic IR Background (CIB), to which they contribute less than 5%. The bulk of the sources contributing to the CIB is thus to be searched for in more distant galaxies, possibly counterparts of the fainter FIRBACK sources still under study. These bright, local, galaxies however play an important role in the evolution of IR galaxies: they dominate the number counts at high 170 μm fluxes, and represent half of the contribution at 250 mJy. Although not particularly massive (typically M^*), they form more stars than a typical spiral galaxy and many are bulge dominated, that could represent the remnant of a former merger. The fainter part of this population may represent the missing link with the higher- z sources found in sub-mm observations.

Key words.**1. Introduction**

The spectral shape of the Cosmic Infrared Background (CIB) detected by the COBE satellite (*FIRAS* experiment between $\sim 150 \mu\text{m}$ and $\sim 1 \text{ mm}$, and *DIRBE* experiment at 100, 140 and $240 \mu\text{m}$) (Puget et al. (1996), see Hauser & Dwek (2002), for a review) indicates a peak at $\sim 150 \mu\text{m}$ with his energy density at least comparable to the optical/UV background. This peak arises from absorbed optical/UV radiation from star formation and AGN activity in obscured galaxies, that is re-radiated in the far-infrared. This obscured population of galaxies could host approximately half of the massive star formation activity over the history of the Universe (e.g Flores et al. 1999).

Together with the Lockman Hole survey (Kawara et al. (1998)), the FIRBACK survey (Dole et al. 2001) was the most reliable and deepest ($\sigma(170 \mu\text{m}) \sim 45 \text{ mJy}$) infrared census at wavelengths between $20 \mu\text{m}$ and $850 \mu\text{m}$, and the only far-infrared survey with a better sensitivity than IRAS, until *SPITZER* observations become available. It is close in wavelength to the peak of the CIB seen by COBE, and because of this wavelength proximity, characterizing the FIRBACK sources is an essential step towards understanding the nature of the sources that generate the CIB.

The FIRBACK survey used about 150 hours of ISO observing time, corresponding to one of the largest ISO programs (Kessler et al. 2000). It covers about 4 square degrees in three high galactic latitude fields, called FIRBACK South-Marano (FSM), FIRBACK North 1 (FN1) and FIRBACK North 2 (FN2). The northern fields observed in FIRBACK are a subset of the larger area covered by the ELAIS survey at shorter wavelength (Oliver et al. 2000). The precise location of the fields, the details of the reduction process, an assessment of the reliability of the detected individual sources, as well as the positions of the close to 200 sources detected with flux $S > 135 \text{ mJy}$ (the 3σ limit) are given in Dole et al. 2001. Our knowledge of these sources is still quite limited. Patris et al. (2003) have published spectra of the 21 brightest FIRBACK sources in the southern FSM field. These bright sources are mostly nearby ($z < 0.2$) dusty star forming galaxies. They exhibit star formation rates of a few tens of solar masses per year with typical IR luminosities of about $10^{11} L_{\odot}$. The fraction of Active Galactic Nuclei (AGN) is low, around 15% at most. In the north, two optical sources ($I = 24$ & 22) were observed in FN1 with ESI on Keck, revealing higher redshift objects ($z = 0.5$ and 0.9 , respectively (Chapman et al. 2002). These two sources are identified as UltraLuminous IR galaxies (ULIRG's), with merger morphologies and relatively cold dust temperatures.

Send offprint requests to: dennefel@iap.fr

* Visiting Astronomer, Observatoire de Haute-Provence, CNRS, France

Finally, based on a statistical analysis (Sajina et al. (2003)), the FN1 sources appear to show a bimodal redshift distribution, with normal star-forming galaxies at $z \simeq 0$ and a tail of a much more luminous galaxy population at $z \sim 0.4-0.9$.

In this paper, we present the information available in the FN1 field, for all FIRBACK sources with flux $S > 4\sigma$ ($=185$ mJy) and give some insights on the fainter flux population. The detailed analysis of all the FIRBACK population is not complete up to now: the identification process is a long process which requires many complementary observations in various wavelength ranges. This paper describes the currently available data in this N1 field, thus allowing the community to conduct complementary follow-up observations if appropriate. Emphasis is put on the brighter (thus presumably closer) sources where the identification is secure. Work is continuing on those sources with multiple or fainter optical counterparts, which probably represent a population further away.

The paper is organised as follows. The complementary observations available to date are presented first (Sect. 2). Then, we describe the identification process and give the results source by source (Sect 3.). In Sect. 4 and 5, we discuss the optical and IR properties of our sample. The IR/radio correlation is discussed in Sect. 6, and in Sect. 7, we analyse the star formation rates. We finally give some global properties for the population of sources with fluxes between 3σ and 4σ in Sect. 8 and discuss all the results in the last section (Sect. 9).

2. Complementary observations

The FN1 field has been covered (sometimes in part only) by radio, millimeter, sub-millimeter, 90, 15 and 6.7 μm , observations, U, g', r', i', Z and K-band imaging and visible spectroscopy. In this section, we describe briefly all these data and their relevance for the present analysis.

2.1. The ELAIS observations

The European Large Area ISO Survey (ELAIS) has surveyed a total of 12 square degrees at 15 μm using the ISOCAM instrument (Cesarsky et al. 1996) and at 90 μm using ISOPHOT (Lemke et al. 1996). Seven square degrees have also been covered at 6.7 μm , but only one square degree at 170 μm (the FN2 field). The ELAIS final band-merged catalog has recently become available (Rowan-Robinson et al. 2004).

The FIRBACK-FN1 field discussed here has been covered at 170 μm over two square degrees in an additional observing run conducted during the "supplementary" lifetime of the ISO satellite. For association of FIRBACK sources in the FN1 field with shorter wavelength data, only the ELAIS data at 15 μm have been used, as it is the only wave-

length where the field coverage is nearly complete. In general, we prefer not to use the 90 μm catalogue (Heraudeau et al. 2004) since it is clearly incomplete, although, in some cases, positions of 90 μm sources with high fluxes have been used to make the identification process converge. Since the ELAIS survey is a shallow survey, the sensitivity at 15 μm is limited by the instrumental noise. The catalogue of Vaccari et al. (2005) (<http://astro.imperial.ac.uk/~vaccari/elais>), which is used here, has a completeness limit at the faint end of about 1 mJy at 15 μm , with a 1σ photometric error better than 0.25 mJy. It provides a source density of about 170 sources per square degree on average, down to the 5σ limit, to ease the FIRBACK identifications. Its rather low sensitivity biases the 15 μm detections towards the lowest redshift sources, but corresponds well to the brightest FIRBACK population.

2.2. The radio data

The Very Large Array (VLA) has been used by Ciliegi et al. (1999) in C configuration to carry-out a sensitive 20-cm radio survey of the FN1, N2/ELAIS and N3/ELAIS fields. In the FN1 field, the flux limit varies over the area surveyed: a circular central region with a flat noise distribution ($\sim 200 \text{ arcmin}^2$, $5\sigma=0.135 \text{ mJy}$), surrounded by concentric annular regions, where the noise increases for increasing distance from the centre (the last annulus has a 5σ rms noise of 1.15 mJy). These regions of the sky had also been surveyed previously to shallower flux limits at 20cm, in the NVSS survey in the VLA D configuration (Condon et al. (1998)) and the FIRST survey in the VLA B configuration (Becker et al. (1995)).

For the identification process, we use both the 5σ radio catalogue of Ciliegi et al. (1999) and the FIRST catalogue. When no radio source is found in the FN1 position error circle, we go back to the radio map to compute 5σ upper limits and search for radio sources down to the local 3σ noise value. Within the error circles of the 56 brightest FIRBACK FN1 sources, we found at least one radio source for 30 of them. Eight of those have their radio flux in the $3 < S < 5\sigma$ range, and three have been found in the FIRST catalogue. When the FN1 source position is outside the Ciliegi et al. (1999) coverage, a 5σ upper limit from the FIRST survey is used.

2.3. Millimeter and sub-millimeter data

IRAM 1.3 mm observations have been conducted with MAMBO on some (~ 10) radio positions that were coincident with FIRBACK positions. Only 2 or 3 sources seem to be detected. The data are currently under analysis and will not be used in this paper.

On the sub-millimeter side, early observations of some FIRBACK sources were published by Scott et al. (2000), followed by observations of a sample of 30 FIRBACK N1 sources by Sajina et al. (2003). This sample as a whole (co-adding all the data for all the observed sources) is detected at the 10.6σ level at $850\ \mu\text{m}$ and at the 9.0σ level at $450\ \mu\text{m}$ ($\langle S_{850} \rangle = 2.5 \pm 0.2\ \text{mJy}$ and $\langle S_{450} \rangle = 16.7 \pm 1.9\ \text{mJy}$). Out of the 30 N1 sources, 7 are detected at the $>3\sigma$ level at $850\ \mu\text{m}$ (3 of them have $3\sigma < S < 4\sigma$) and 5 sources are detected at the $>3\sigma$ level at $450\ \mu\text{m}$. Only these $S > 3\sigma$ detections will be used here.

2.4. X-ray data

A cross-correlation between the ELAIS-ISO $15\ \mu\text{m}$ survey and the ROSAT all-sky survey has been conducted by Basilakos et al. (2002). Three sources were found, corresponding roughly to the fields of the $170\ \mu\text{m}$ sources FN1-35, 126 and 295. But the position of the X-ray source is in these 3 cases always at more than $140''$ from the centroid of the PHOT source, and is therefore largely outside our error circle. We can therefore conclude that there is no association of a $170\ \mu\text{m}$ source with an X-ray source, at the sensitivity level of the Rosat all-sky survey.

Another cross-correlation of the $15\ \mu\text{m}$ survey with specific Chandra pointings in the N1 (and N2) field has been performed by Manners et al. (2004). Three matches were found in N1, but none correspondings to a FIRBACK source (except perhaps *FN1 – 042*, see the discussion of individual sources).

2.5. Other IR data.

We derived IRAS 60 and $100\ \mu\text{m}$ fluxes (or upper limits) for each FN1 source position, by using SCANPI¹, a tool developed for visualizing, plotting and averaging calibrated IRAS survey scans. Each FN1 source was checked by eye. For point sources with signal-to-noise greater than 3, we determine the flux by fitting the point source template. When no clear detection was obtained, a 3σ upper limit was set. The whole procedure is fully described at: <http://irsa.ipac.caltech.edu/IRASdocs/scanpi/>. None of the identified FIRBACK galaxies is resolved by IRAS. We checked that the fluxes derived by using SCANPI (in and near the FIRBACK fields) were in good agreement with those of the IRAS Faint Source Catalog for sources in common.

We also searched for associations of optical counterparts with 2MASS (Kleinmann et al. (1994)) sources and an association was found in the Extended Source Catalogue (XSC) in most cases. Although several magnitudes and colours are usually available, we have extracted only the total K_s magnitude: we do indeed not

¹ <http://irsa.ipac.caltech.edu/applications/Scanpi/>

intend to use the near-IR colours to fit the spectral energy distributions (in view of the probable complex stellar populations content), but simply use the K luminosity to estimate the mass of the galaxy. In a few cases when no 2MASS magnitude was available, we used K magnitudes from the work of Sajina et al. (2003).

The N1 field is one of the fields of the SWIRE legacy survey (Lonsdale et al. (2003)) using the SPITZER satellite (Werner et al. (2004)) and is the first one to have been observed. The products (Version 1.0) comprise images and catalogues in the four IRAC bands (3.6, 4.5, 5.8 and 8.0 μm) and three MIPS bands (24, 70 and 160 μm), described by Surace et al. (2004) on the Spitzer Web site (<http://ssc.spitzer.caltech.edu/legacy/>), and were released on Oct. 27, 2004, after this paper was first submitted. The use of those data for the analysis of FIRBACK sources is thus deferred to a subsequent paper. We note however that the available MIPS 160 μm catalogue contains 178 entries down to the cut-off limit of 200 mJy, in an area of 8.5 square degrees. Twenty-five of them only lie within the smaller FN1 area, to be compared to 44 FIRBACK sources down to the same flux limit (at 170 instead of 160 μm). We have however checked on the SWIRE 160 μm images that all the FIRBACK sources were present down to 200 mJy, and almost all of them (only three possibly suspicious cases) down to 140 mJy, so that all the FIRBACK sources discussed in this paper are real and that the difference in number counts is to be ascribed to incompleteness of the preliminary SWIRE 160 μm N1 catalogue, and probably incomplete field coverage. While the sensitivities of both surveys are therefore comparable, the SWIRE data will later allow a larger sample of presumably similar objects to be studied, with the help of the shorter wavelength data for more precise identifications.

2.6. Optical data

Multicolour photometry was obtained over the FN1 field, in U through Z, as part of the INT Wide Field Survey ² (MacMahon et al. (2001)), with the Wide Field Camera covering about 0.3 deg² at once on the 2.5m Isaac Newton Telescope. The photometry is described in Gonzalez-Solares et al. (2005) and the limiting magnitudes range from ~ 21.9 in Z to ~ 24.9 in g'. The corresponding catalogue was used to search for optical associations with the FN1 sources using the likelihood ratio method, as described most recently in Mann et al. (2002). For each source, the probability P_{ran} is computed that an association with an optical object at the given likelihood ratio has occurred by chance, on the basis of simulations using associations with random positions in the INT data. A low P_{ran} value therefore means a more secure identification. The results of these computations are used together with the 15 μm and 21 cm catalogs to find the best

² <http://www.ast.cam.ac.uk/~mike/casu/WFCsur/WFCsur.html>

identifications (as explained in Sect 3).

DSS2 data were used for initial identification purposes and preparation of the spectroscopic observations, waiting the accessibility of the INT images, and are shown as small charts in Fig. 10.

Optical spectra were taken at the Haute-Provence Observatory (CNRS, France) with the 1.93m telescope during several observing runs between 1999 and 2004. The Carelec long-slit spectrograph was used with a 300 l/mm grating and an EEV CCD detector of 2048x1024 pixels of 13.5 μm each, giving a spectral element of 1.75 \AA per pixel and a spectral resolution of 6.5 \AA with the 2'' entrance slit generally used. The total spectral coverage is about 3600 \AA but the central wavelength was different from one run to another, to allow the H α emission sometimes to be detected in higher redshift objects. The orientation of the slit was adjusted to register more than one object in a given exposure, when adequately bright galaxy candidates were available in the PHOT error circle.

The reduction followed the usual procedure, with flat-fielding, wavelength calibration, and spectral response determination through observations of several standard stars, the master standard usually being BD+26,2606. The relative response is determined with an accuracy of a few percent, the blue part of the spectrum having the poorest correction due both to the decreasing response of the detector and the average extinction curve available. Absolute fluxes are available only part of the time, due to changing weather conditions: when they are, their accuracy is estimated to be better than 15%, not taking into account light losses at the entrance slit. As these fluxes are only indicative, no correction for those losses has been attempted.

3. Identifications: method and results

As the FIRBACK position error circle (Dole et al. 2001) is rather large (100 '' in diameter for a 93% localising probability), the identification process is complex. For the bright PHOT sources (most of those considered in this paper), we selected the bright galaxy (or galaxies) within the PHOT error circle and used, as the major criterion, the distance between the optical galaxy candidate and the centroid of the PHOT detection. If several candidates were possible, the spectral characteristics were then used to identify the good ones: the FIRBACK counterparts are expected, by analogy with IRAS sources, to be primarily starforming galaxies (or AGNs), albeit possibly colder as they are selected at longer wavelengths, and their spectral features should thus be rather similar to the typical objects found in the IRAS survey (e.g. Veilleux et al. (1995) and references therein). The complementary observations with better positional accuracy were used conjointly to find the correct optical association(s) to the far-IR source. We

primarily used the ISOCAM 15 μm and/or the radio 21 cm data. The ratio of sensitivity between ISOCAM at 15 μm (which is instrumental noise limited) and ISOPHOT at 170 μm (which is confusion noise limited) is such that it is unlikely that an extragalactic source will be detected at 15 μm without contributing significantly to the FIRBACK 170 μm flux (unless it has a very unusual SED). On the other hand, the use of the radio data assumes that the detected sources have a similar radio to far-IR ratio as sources previously detected by IRAS (e.g. Condon & Broderick (1991)). The use of this criterion could prevent the detection of a different type of source in this sample (should they exist), but in practice, at least for the bright optical galaxies observed here, there was in general no ambiguity: the bright galaxy detected closest to the PHOT source indeed had spectral characteristics similar to those of IRAS galaxies; it moreover very often had an associated 15 μm detection so that the use of the radio data was not essential. It will however become important when going to fainter PHOT sources, where more than one, faint, optical counterpart can be located within the error circle.

FIRBACK sources were then distributed in three groups:

1. Identified sources: sources associated with one bright optical galaxy, usually also detected in radio and/or ISOCAM. Fainter optical sources, like FN1-040 (which lies at $z=0.45$), are also put in this category, when the radio/ISOCAM identification was also unambiguous.
2. Multiple sources or uncomplete identification. Into this category are put FIRBACK sources with more than one optical/15 μm /radio counterpart and FIRBACK sources with no secure identification.
3. Unidentified sources. Either no radio or 15 μm source detected to help identification, or the optical galaxies are too faint to be detected spectroscopically with the available instrument. We cannot reach a conclusion in such cases.

Out of the 56 ISOPHOT sources in the 4σ sample, 28 are fully identified, 17 have multiple or incomplete identifications and 11 sources have no identified counterpart. We comment on a few sources in the $3 < S < 4\sigma$ range, which were also analysed. Fig. 10 presents the DSS images with the FIRBACK error circle and the radio and ISOCAM counterparts when present.

3.1. Identified sources

This section gives details concerning the identified sources. We emphasize the complementary data (near-IR or radio) when they are important to secure the identification. For all sources, fluxes in the various bands (IR and radio) and far-infrared colors are given in Table 1. Optical properties are given in Table 2 and spectral characteristics are given in Table 4.

FN1 – 000: Identification with a bright optical galaxy, also detected at 15 and 90 μm . This galaxy is a merger, with clear tidal tails. The two other bright objects inside the PHOT error circle are stars.

FN1 – 001: Bright optical galaxy.

FN1 – 002: Bright optical galaxy, also detected at 90 μm .

FN1 – 003: Bright optical galaxy with 15 μm emission. This identification has a higher P_{ran} probability to occur by chance, because the galaxy is located $\approx 30''$ from the ISOPHOT centroid but there are no other obvious identifications on the image. This source is detected by IRAS at 100 μm only (upper limit at 60 μm , although this band is more sensitive) and should therefore be a rather cold galaxy. The spectrum shows a low equivalent width of $\text{H}\alpha$, suggesting a weak starburst in an older galaxy.

FN1 – 004: Bright optical galaxy with a point-like nucleus. This source is also detected by SCUBA at 450 μm (32.5 ± 7.1 mJy). Its spectrum reveals a Seyfert 2 type (strong, narrow [NII] lines). A fainter galaxy at the southern edge of the error circle has a similar redshift and also $\text{H}\alpha$ emission, but is not detected in radio nor at 15 μm : it is unlikely to contribute much to the far-IR flux.

FN1 – 005: Faint optical galaxy with 15 μm detection. The identification has a higher P_{ran} value, because the galaxy is located $\approx 30''$ from the ISOPHOT centroid, but the ISOCAM identification is unambiguous. This object has been observed in the optical with the Palomar200/DoubleSpec instrument (Chapman, private communication).

FN1 – 006: bright optical galaxy detected at 15 μm and 90 μm . Because of its location $\approx 30''$ away from the PHOT centroid, this identification would have a higher probability of occurring by chance, but the spectrum is typical of a reddened starburst. The bright object just east of the galaxy is apparently a star. A second 15 μm source, much fainter (a factor of about 6) than the other one, is also located within the error circle, but does not show any obvious optical counterpart. In view of its faintness, and because it does not correspond to the 90 μm source, it is unlikely to contribute much to the 170 μm flux.

FN1 – 007: Bright optical galaxy with 15 μm , and 1.4GHz emission. This source is detected by SCUBA both at 850 μm and at 450 μm (23.4 ± 8.1 mJy for the latter). It has a very cold IRAS colour, but does not lie in the few, very faint, well identified cirrus filaments in the N1 field, so is unlikely to be contaminated by background.

FN1 – 009: Identification with a bright optical galaxy with 15 μm and 1.4GHz emission. The spectrum, although dominated by stellar features, shows clearly the presence of an active nucleus (strong [OI], large [NII]/ $\text{H}\alpha$ and [SII]/ $\text{H}\alpha$ ratios), classified as Sey2. The bright object at the southern edge of the PHOT error circle, with a 15 μm detection, is a spectroscopically confirmed cold star.

FN1 – 011: bright optical galaxy with a 15 μm detection. The other bright object to the SW is a star.

FN1 – 012: Bright optical galaxy detected at 15 μm and 90 μm . Although the galaxy is $\approx 30''$ from the ISOPHOT centroid, the identification is secure, with a typical reddened starburst spectrum.

FN1 – 014: This source does not have 1.4GHz data (it lies outside the VLA surveyed area) but has a clear 15 μm counterpart and is also detected at 90 μm . The optical objects were however too faint to be observed spectroscopically with our equipment. A photometric redshift has been provided by T. Babbedge (private communication).

FN1 – 015: This source is identified with a bright optical galaxy with 1.4GHz emission, and SCUBA detection. It has one of the highest redshifts measured in our sample, so that $\text{H}\alpha$ falls outside our prime spectral range.

FN1 – 016: Identification with a bright optical galaxy detected at 15 μm , and 1.4GHz. This source is detected by IRAS at 60 and 100 μm , and by SCUBA both at 450 and 850 μm . Although its position is rather offset with respect to the PHOT centroid, the identification seems to be fairly secure, in view of the detection in all these wavebands, and its typical reddened starburst spectrum.

FN1 – 018: bright optical galaxy with 15 μm detection but no radio emission. Its spectrum, with a strong $[\text{NII}]/\text{H}\alpha$ ratio, indicates the presence of an AGN.

FN1 – 020: Identification with a faint optical galaxy also detected at 15 μm . This source is detected by IRAS at 100 μm only, and is thus presumably cold. We could not secure an optical spectrum, but a photometric redshift has been provided by T. Babbedge (private communication). The other bright object in the error circle seems to be a star.

FN1 – 021: bright optical galaxy also detected at 15 μm . A second galaxy, at the eastern edge (but outside, at $69''$) of the PHOT error circle, also detected at 15 μm , with a starburst-type spectrum and a velocity close to the bright galaxy one, might also contribute to the detected far-IR flux.

FN1 – 023: bright optical galaxy with a 15 μm detection, but not detected by IRAS. The bright object NE of the galaxy is starlike.

FN1 – 024: Bright optical galaxy with 15 μm and 1.4GHz emission and a starburst spectrum. Although there are other, fainter galaxies in the field (but not detected in radio nor in mid-IR), this source is considered as the main contributor to the far-IR emission.

FN1 – 026: Identified with an optical galaxy having also 15 μm and 90 μm detections, but no radio detection. The other two bright objects in the error circle are presumably stars.

FN1 – 031: Identified with an optical galaxy with 90 μm and 1.4GHz detections. This source is also detected by SCUBA at 850 μm .

FN1 – 033: Identified with a faint optical galaxy with 15 μm emission, but no radio detection.

FN1 – 035: Optical galaxy with also a 15 μm detection but no radio detection (2MASS

detection, galaxy classified as IrS).

FN1 – 038: The faint optical galaxy inside the error circle displays emission lines in its spectrum and is associated with a 15 μm source. A radio source exists, with no obvious optical counterpart, but lies outside the error circle and is therefore not associated with the PHOT source.

FN1 – 039: Identified with a faint optical galaxy detected at 1.4GHz. This source is also detected by SCUBA at 450 μm , and has been spectroscopically observed with the Palomar200/DoubleSpec instrument (Chapman, private communication).

FN1 – 040: Identified with a faint optical galaxy detected at 1.4GHz and with SCUBA at 850 μm . The bright object in the center of the error circle is a star. This is one of the 2 higher redshift FIRBACK sources detected by Chapman et al. (2002), who note it is an interacting pair.

FN1 – 041: Identified with a bright galaxy in the center, detected in radio and in mid-IR, with a typical emission-lines spectrum.

FN1 – 043: Identified with an optical galaxy, also detected at 15 μm . A high [NII]/H α ratio indicates an active nucleus, but the S/N of the spectrum is insufficient to distinguish between a liner or a reddened Sey2.

3.2. Multiple or incomplete identifications

We detail in this section the FIRBACK sources with more than one possible identification and/or a non-secure identification.

FN1 – 008: Two sources with 1.4GHz emission within the error circle. The brightest optical counterpart is at $z=0.26$ and has a 350 μm CSO detection. It shows a reddened spectrum with absorption features due to hot stars, but H α is unfortunately out of our spectral range. The faintest galaxy (the second radio source) has a SCUBA measurement and a K-band magnitude of 14.2 (Sajina et al. 2003)

FN1 – 010: This source has two 15 μm counterparts associated with bright optical galaxies. It is also detected by IRAS at 60 μm . The bright galaxy in the error circle has a reddened continuum with strong stellar absorption features, and H α and [NII] emission of small equivalent width. The [NII]/H α ratio clearly indicates an AGN, but the non-detection of the emission features in the blue spectral range does not allow us to distinguish between its being a Sey2 or a Liner. The fainter galaxy within the error circle is detected in radio at 1.4GHz and also at 15 and 90 μm (while the bright galaxy is not), but was too faint to be observed spectroscopically here. The identification of the PHOT source is therefore still uncertain, and the far-IR flux may in fact be due to contributions of both galaxies.

FN1 – 017: This source has a 15 μm counterpart associated with a faint galaxy located

at the edge of the error circle. Many other faint galaxies are visible in the error circle, but they were all too faint to be observed here.

FN1 – 019: Two possible counterparts: one bright optical galaxy with 15 and 90 μm emission, whose spectrum indicates the possible presence of a Liner (the emission lines have also a small equivalent width). And one fainter galaxy with 1.4 GHz emission ($3\text{-}5\sigma$ detection), but no available spectrum.

FN1 – 025: Two bright galaxies in the error circle display emission lines in their spectrum, but are not related to each other. One has a 15 μm counterpart. A fainter galaxy in the field, this one with 1.4 GHz emission ($3\text{-}5\sigma$ detection), could not be observed spectroscopically. The situation is complex, as all three galaxies may contribute to the far-IR flux.

FN1 – 029: This source could be identified with an optical galaxy close to the PHOT centroid and both 15 μm and 1.4 GHz detections. Another faint, optical galaxy, also with 1.4 GHz emission, lies however at the border ($51''$) of the error circle (not observed spectroscopically) and could contribute also to the far-IR emission.

FN1 – 032: A bright galaxy with 15 μm counterpart, close to the PHOT centroid, displays weak emission lines superposed on a strong, reddened, stellar continuum. The $[\text{NII}]/\text{H}\alpha$ ratio, close to 1, indicates the presence of an active nucleus. The 1.4 GHz emission is however associated with another, faint optical galaxy, also close to the center of the error circle, but which was too faint to be observed spectroscopically here.

FN1 – 034: The bright galaxy close to the PHOT centroid displays emission lines in its spectrum, has 15 μm emission but no radio counterpart. It is also detected by IRAS at both 60 and 100 μm . The radio 1.4GHz emission in this field corresponds to a very faint optical galaxy ($K=19.3$), with a SCUBA detection at 450 μm (but not at 850 μm), which could not be observed spectroscopically.

FN1 – 037: faint optical galaxy, with also a 15 μm detection. Could not be detected spectroscopically. Another 15 μm source, inside the error circle, is associated with an even fainter galaxy.

FN1 – 042: The bright optical galaxy close to the center (detected in mid-IR but not in radio) shows only weak emission lines in its spectrum and is unlikely to be the real counterpart. Three radio sources are detected in the vicinity, two inside the error circle, associated with faint galaxies which could not be observed in the optical, and correspond probably to the emitters of the far-IR flux. The third, south-eastern, radio-source is slightly outside the PHOT error-circle and corresponds to one of the X-rays sources found by Manners et al. (2004): they do classify this object as starburst-galaxy, and it could contribute also to the far-IR flux.

FN1 – 044: A comparatively bright optical galaxy, detected in radio at 1.4 GHz, and also at 15 μm and 90 μm with ISO and 60 μm with IRAS, is undoubtedly a counterpart to the 170 μm source. Its spectrum indicates the presence of an AGN (liner or Sey2).

One other radio source is however also present within the error circle, and is associated with a very faint optical galaxy, which could contribute also to the far-IR emission.

FN1 – 045: The bright galaxy, with radio emission (and a 2σ SCUBA detection) is the probable identification. However, there are other, fainter galaxies with unknown properties in the field.

FN1 – 046: Two bright galaxies are close to the border of the FIRBACK error circle. The one inside, with no radio emission but 15 μm emission, is a standard emission line galaxy which would be considered as the far-IR counterpart if it would be alone. The second galaxy, just outside the error circle, does however not show emission lines. There is moreover another 15 μm source lying in the error circle. This source is associated with a very faint optical galaxy. The identification is therefore not complete here.

FN1 – 048: A bright galaxy, with emission lines, is situated close to the center of the error circle. Two radio sources, however, are also present (closer to the boundary), one superposed on a bright star (spectroscopically confirmed as late type), the other on a very faint optical galaxy. This latter source is also detected by SCUBA both at 450 and 850 μm , and is likely also to be a contributor to the far-IR source.

FN1 – 049: A bright optical galaxy detected at 15 μm and at 1.4 GHz ($3\text{--}5\sigma$ detection) is certainly a contributor to the far-IR source. In the error circle lies another 15 μm source associated with a very faint optical object.

FN1 – 050: Two 15 μm sources are detected at the limit of the error circle. They are both associated with very faint optical galaxies.

FN1 – 053: One 15 μm source is detected at the border of the error circle (at 49.7 arcsec). It is associated with a very faint optical galaxy which could not be observed spectroscopically.

ID	ISO 15 μm	IRAS 60 μm	IRAS 100 μm	ISO 170 μm	SCUBA 850 μm	VLA 1.4 GHz	100/60	170/100
FN1-000	27.42 \pm 4.17	620 \pm 28	820 \pm 63	837.7 \pm 89.7		4.10 ^F \pm 0.15	1.32	1.02
FN1-001	17.45 \pm 2.68	260 \pm 31	410 \pm 99	597 \pm 72.5	6.1 \pm 1.6	0.74 \pm 0.23	1.58	1.46
FN1-002	11.67 \pm 1.87	160 \pm 25	340 \pm 93	544.5 \pm 68.8	4.4 \pm 1.1	0.64 \pm 0.04	2	1.6
FN1-003	8.94 \pm 1.37	< 100	220 \pm 60	408.3 \pm 59		<0.75	>2.2	1.86
FN1-004	11.38 \pm 1.85	100 \pm 22	300 \pm 73	390.8 \pm 57.7	3.6 \pm 1.4	0.88 \pm 0.10	3.0	1.3
FN1-005	4.15 \pm 0.65	110 \pm 34	300 \pm 78	373.8 \pm 56.6		<1.00 ^F	2.74	1.25
FN1-006	11.6 \pm 1.78	100 \pm 29	300 \pm 82	347.6 \pm 54.7		<1.00 ^F	3	1.16
FN1-007	5.74 \pm 0.9	70 \pm 25	520 \pm 90	337.6 \pm 54	4.4 \pm 1.6	1.04 \pm 0.10	7.4	0.65
FN1-009	5.71 \pm 0.88	<90	< 400	313.1 \pm 52.3	3.5 \pm 1.5	1.15 \pm 0.07		>0.78
FN1-011	2.78 \pm 0.47	<78	<255	304.5 \pm 51.6		<1.00 ^F		>1.19
FN1-012	3.93 \pm 0.61	90 \pm 34	<400	302.1 \pm 51.4	1.5 \pm 1.6	0.31 \pm 0.07	<4.44	>0.76
FN1-014	2.84 \pm 0.48	150 \pm 19	380 \pm 57	295.2 \pm 50.9		<1.00 ^F	2.53	0.78
FN1-015	2.9 \pm 0.48	<78	<300	294.4 \pm 50.9	1.4 \pm 1.6	0.52 \pm 0.07	>3.77	>0.98
FN1-016	7.87 \pm 1.20	160 \pm 17	360 \pm 92	289.3 \pm 50.5	1.5 \pm 1.2	1.55 \pm 0.07	2.25	0.8
FN1-018	2.77 \pm 0.46	<105	<210	287.8 \pm 50.4		<1.00 ^F		>1.37
FN1-020	2.05 \pm 0.37	< 108.	230. \pm 76	283.40 \pm 50.1		< 0.5	>2.62	1.23
FN1-021	2.98 \pm 0.35	130 \pm 26	<360	271.3 \pm 49.2		< 0.75	< 2.77	>0.75
FN1-023	3.44 \pm 0.55	< 69	<294	269.9 \pm 49.2		<1.00		> 0.92
FN1-024	5.02 \pm 0.78	<84	<147	266.2 \pm 48.9	2.3 \pm 1.3	0.75 \pm 0.04		>1.81
FN1-026	9.16 \pm 0.23	< 66	<243	240.6 \pm 47.1		<1.00		>0.99
FN1-031	3.74 \pm 0.59	<69	<237	225.2 \pm 46	1.9 \pm 1.1	0.43 \pm 0.04		>0.95
FN1-033	3.62 \pm 0.43	< 90.	< 330	224.1 \pm 45.9		< 0.5		>0.68
FN1-035	4.22 \pm 0.67	< 63.	< 192	218.2 \pm 45.5		<0.75		>1.14
FN1-038	2.17 \pm 0.38			206.9 \pm 44.7		<1		
FN1-039		< 57	<246	205.2 \pm 44.5	-0.1 \pm 2.3	0.58 \pm 0.05		>0.83
FN1-040		< 75.	< 153	204.7 \pm 44.5	5.4 \pm 1.1	0.33 \pm 0.03		>1.34
FN1-041	4.50 \pm 0.72	<69	<243	204.2 \pm 44.5	-0.1 \pm 2.5	0.76 \pm 0.04		>0.84
FN1-043	2.47 \pm 0.4	< 78	<225	200.6 \pm 44.3		<0.75		>0.89

^F : FIRST radio survey

Table 1. Infrared and radio data (all in mJy) for the FIRBACK identified sources, together with infrared colors.

3.3. Unidentified sources

For all these sources (except 4), there is no radio or ISOCAM detection inside the PHOT error circle, and no obvious galaxy counterpart. For sources *FN1* – 022, *FN1* – 027, *FN1* – 051, *FN1* – 054, *FN1* – 055, we have no further information to give. The 6 last sources are:

FN1 – 013: There is a mid-IR galaxy ($F_{15}=1.36\pm 0.3$ mJy) associated with a very faint optical galaxy. We have no further information on this object.

FN1 – 028: Two bright optical galaxies, one at the edge (SE) of the error circle and one well inside (NW) have been observed spectroscopically. They have recession velocities of 19921 and 19816 km/sec respectively, but do not display emission lines. There is no radio nor 15 μm detection to help identification, and the two optical galaxies are unlikely the sources of the far-IR emission.

FN1 – 030: The only bright optical source in the error circle is a spectroscopically confirmed star.

FN1 – 036: One ISOCAM position corresponds to a very bright star. Other bright objects seen in the error circle could also be stars (like the other 15 μm faint source).

FN1 – 047: Only stars are seen inside the error circle, the brightest one being also an ISOCAM 15 μm source.

FN1 – 052: This source has one radio counterpart (with radio detection above 3 sigma) but no clear optical identification.

3.4. Some sources fainter than the 4σ limit

For the fainter ISOPHOT flux galaxies (47 sources, $3\sigma < S < 4\sigma$), radio and mid-infrared counterparts may be expected to become rarer. However, this is only marginally the case. The ISOPHOT sources without any radio and mid-IR counterparts represent 23% of the $S > 4\sigma$ sample and 34% of the $3\sigma < S < 4\sigma$ sample. Among the 47 ISOPHOT sources with fluxes between 3 and 4σ , 12 have a 15 μm counterpart, 12 have a radio counterpart and 7 have both. This tends to show that the catalog is reliable down to the 3σ level. Two examples were observed optically:

FN1 – 057: A bright galaxy inside the error circle is also detected at 15 μm . It displays emission lines and is the likely identification. The source is also strong at both 60 and 100 μm (IRAS detection).

FN1 – 101: Bright galaxy with emission lines, close to the center of the error circle, also detected at 15 and 90 μm . It also coincides with the only radio source in this field, and is therefore the obvious identification of this much fainter 170 μm source.

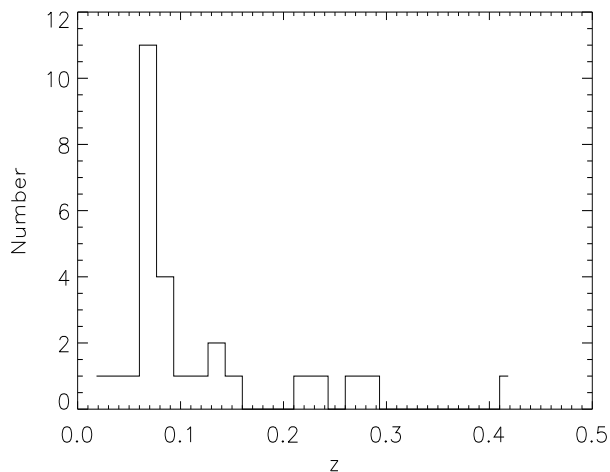


Fig. 1. Redshift distribution of the 28 FIRBACK fully identified sources.

In all the following (except when specifically mentioned), we discuss only sources with secure identifications (28 sources).

4. Optical properties of identified sources

4.1. Optical colors and morphologies from the INT-WFC survey

FIRBACK sources have been observed as part of the INT Wide Field Survey in the U, g' , r' , i' and Z filters. INT photometric bands are similar to the SDSS bands (Sloan Digital Sky Survey (Fukugita et al. 1996), see the WFS section for further details (Sect. 2.6).

The morphology of all the objects in our sample was assessed visually on the i' images, using the common Hubble sequence as in Postman et al. (2005). With the Advanced Camera for Surveys (ACS) on the Hubble Space Telescope, a visual classification of that kind has a typical random error of 25%, which can be reduced to 6% when only two broad categories are used (early-type, and spirals/irregulars). Although we used ground-based images here, the objects are all relatively close so that the uncertainty in classification is of the same order of magnitude.

Optical colors were derived for identified sources and they are given in Table 2. The source *FN1 – 040* is too faint for precise photometry and *FN1 – 000* does not have a g' magnitude. They are both excluded from the following analysis. The $(g' - r')$ and the $(U - r')$ color histograms are shown in Fig. 2. Strateva et al. (2001) have found, from the analysis of about 150000 galaxies in the SDSS, that the distribution of galaxies in $(U - r')$ is strongly bimodal with an optimal color separator of $(U - r') = 2.22$ for low redshift ($z < 0.4$) objects: late type galaxies lie mostly on the blue side, with $(U - r') < 2.22$. Although selected from the far-IR, most of our galaxies lie also on the blue side: this is coherent with their classification as late-type for most of them, but suggests that

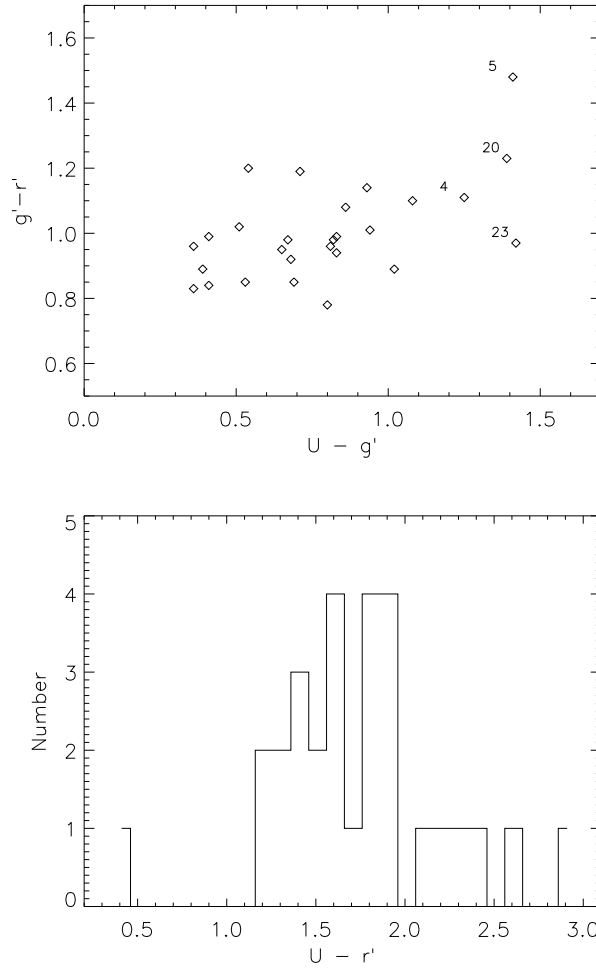


Fig. 2. Optical colors of the identified sources. At the top, we show the $(g' - r')-(U - r')$ colour-colour diagram, while the bottom gives the $(U - r')$ histogram.

they are not heavily obscured, at least outside the central regions. The reddest sources ($(U - r') > 2.2$; FN1-04, FN1-05, FN1-20, FN1-23) are also spiral galaxies, but this time probably affected by heavier extinction.

These measurements have not been corrected for galactic extinction, but this correction should be negligible in such low HI-column density field as the N1 field ($N_{\text{HI}} = 10^{20} \text{ at/cm}^2$).

Uncertainties on the magnitudes are smaller than 0.1 mag.

ID	Position (J2000)	P_{ran}	r' Mag.	(U-r')	(U-g')	(g'-r')	K_s mag	Morphology	Comments
FN1-000	160552.8+540651	0.07	17.94			1.46	13.41 \pm 0.13	Irregular	Merger with tail
FN1-001	160736.6+535730	0.00	16.67	1.28	0.39	0.89	12.29 \pm 0.09	Sb/c	
FN1-002	161005.8+541029	0.10	17.73	1.6	0.68	0.92	12.63 \pm 0.11	Sb/c	
FN1-003	161254.1+545526	0.29	17.13	1.94	0.86	1.08	12.57 \pm 0.09	Sa	Em. with small EW
FN1-004N	161109.5+535808	0.01	16.84	2.36	1.25	1.11	11.80 \pm 0.07	Sa/b	Star forming knots (Seyfert)
FN1-004S	161107.3+535711	1	19.03	1.59	0.74	0.85		Sa/b	
FN1-005	160443.4+543331	0.84	19.22	2.89	1.41	1.48		2 Spirals	Merger
FN1-006	160433.9+544432	0.32	17.26	1.77	0.83	0.94	12.79 \pm 0.10	Sa/O	
FN1-007	161331.2+541630	0.03	17.18	1.91	1.02	0.89	12.64 \pm 0.09	SO/a	
FN1-009	160803.7+545302	0.01	16.58	1.58	0.80	0.78	11.88 \pm 0.07	Sa	Liner
FN1-011	160808.6+535242	0.13	17.84	1.77	0.81	0.96	13.21 \pm 0.16	Sa	
FN1-012	161214.0+540833	0.30	17.88	1.38	0.53	0.85	13.69 \pm 0.18	Sb	
FN1-014	161551.4+541536	0.43	19.20	1.32	0.36	0.96		Sa/b	
FN1-015	160724.7+541212	0.37	18.89	1.53	0.51	1.02	14.8 \pm 0.1 ^a	Sa/b	
FN1-016	16-738.0+544602	0.97	17.09	1.80	0.82	0.98	13.14 \pm 0.10	Elliptical	
FN1-018	161407.1+541920	0.87	18.92	2.18	1.08	1.1	13.31 \pm 0.20	Sa/b	Edge-on (AGN)
FN1-020	160812.3+545526	0.88	19.72	2.62	1.39	1.23		Disk?	Very faint
FN1-021	161308.0+545142	0.33	18.18	1.60	0.65	0.95	13.05 \pm 0.12	Sa/b	
FN1-021B	161319.2+545137	1	18.04	0.44	-0.10	0.54		E/SO	

^a: K magnitude from Sajina et al. (2003)

Table 2. Photometric properties and morphology of the FIRBACK fully identified sources.

ID	Position (J2000)	P_{ran}	r' Mag.	(U-r')	(U-g')	(g'-r')	K_s mag	Morphology	Comments
FN1-023	160835.4+535020	0.40	18.94	2.39	1.42	0.97	13.63 ± 0.19	Sb/c	
FN1-024	160937.5+541259	0.54	18.36	2.07	0.93	1.14	13.50 ± 0.15	SO	
FN1-026	161436.9+541635	0.27	19.10	1.82	0.83	0.99	13.75 ± 0.18	Sb	Edge-on, dust lanes
FN1-031	161103.7+544322	0.05	17.69	1.25	0.41	0.84	13.36 ± 0.16	SO/a ?	
FN1-033	161301.1+541003	0.22	18.47	1.40	0.41	0.99		E/SO	
FN1-035	161527.7+543414	0.39	18.11	1.65	0.67	0.98	13.38 ± 0.14	Sa/b	
FN1-038	160747.3+534836	0.53	19.26	1.85	0.93	0.92		Sa/b	
FN1-039	160848.9+545151	0.59	20.18	1.90	0.71	1.19	15.8 ± 0.2^a	?	Possibly disk
FN1-041	160814.2+542836	0.30	18.89	1.19	0.36	0.83	14.7 ± 0.1^a	SO/a	
FN1-043	160553.4+542226	0.59	18.69	1.74	0.54	1.20	14.00 ± 0.20	Sb	Barred

^a: K magnitude from Sajina et al. (2003)

Table 2. Photometric properties (continued)...

ID	Position (J2000)	P_{ran}	r' Mag.	(U-r')	(U-g')	(g'-r')	K_s mag	Morphology	Comments
FN1-008	160858.0+541818	0.21	18.83	2.25	0.81	1.44	13.76 \pm 0.19	SO/a ?	Two objects
FN1-010	160930.9+535148	0.26	17.18	2.09	1.04	1.05	12.63 \pm 0.14	Sa/b	Prob. AGN
FN1-019	161235.4+541545	0.01	17.05	1.95	0.94	1.01	12.31 \pm 0.10	Sa/b	AGN
FN1-025N	160833.4+545510	0.88	18.81	1.43	0.64	0.79		Sb/c	
FN1-025S	160834.5+545421	??						Sb	
FN1-028A	160738.2+534250	0.47	17.59	2.04	1.05	0.99	13.68 \pm 0.18	SO/a	
FN1-028B	160746.5+534151	1	16.70	2.20	1.18	1.02	12.26 \pm 0.09	SO	
FN1-029	161117.5+541629	0.26	18.67	2.38	1.38	1.00	13.65 \pm 0.18	Sa/b	
FN1-032	161239.9+543657	0.07	17.38	2.33	1.34	0.99	12.07 \pm 0.08	Sa	AGN
FN1-034	160724.2+544330	0.33	18.66	0.90	0.19	0.71	19.3 \pm 0.8 ^a	Sa/b	
FN1-037	161509.0+541837	0.36	19.42	1.88	1.14	0.74		Sb	Id. uncertain
FN1-042	161038.9+543628	0.08	17.24	2.24	1.35	0.89	12.06 \pm 0.08	Sb	AGN
FN1-044	160931.6+541827	0.74	18.69	1.99	0.93	1.06		Sa	
FN1-045	160853.9+544735	0.6	19.24	2.12	1.11	1.01	14.33 \pm 0.17	Sa	
FN1-046A	161249.4+540837	1	18.01	2.44	1.22	1.22	13.19 \pm 0.13	SO/a	Radio source
FN1-046B	161251.1+540801	0.52	17.38	1.61	0.68	0.93	13.09 \pm 0.12	SBa	Barred
FN1-048	161059.1+542305	0.64	19.37	1.31	0.44	0.87	19.3 \pm 0.9 ^a	Sb/c	
FN1-049	160801.6+543642	0.54	18.89	1.54	0.69	0.85	13.73 \pm 0.20		
FN1-057	160801.6+543643	0.78	18.43	1.64	0.69	0.95	13.26 \pm 0.15	SBa	Barred
FN1-101	160946.1+542127	0.11	18.44	0.85	0.25	0.60		Sa/b	

^a: K magnitude from Sajina et al. (2003)

Table 3. Photometry of additional sources (sources with multiple or uncomplete identification); or sources outside the 4σ sample (FN1-057 and FN1-101).

4.2. Spectral properties

Most of the spectra display both emission and absorption lines. All lines have been used to derive the redshift (except those with low signal to noise ratio, indicated in brackets in Table 4 and in Table 5). The 1σ dispersion is given after the velocity: it should be smaller when more lines are available, but the well-known systematic difference between emission and absorption lines also affects the result when both types of lines are used. To this internal error has to be added the (random) external error, which should not exceed one pixel after correction for flexures, so that the final uncertainty in velocities should be better than 150 km/s in most cases. The distribution in redshifts of the identified sample is plotted in Fig. 1. Out of the 28 identified sources, about 80% have redshifts lower than 0.25. This is in very good agreement with the redshift distribution of the Lagache et al. (2003) model of evolution of IR galaxies.

The emission line spectra are very similar to those of standard IRAS galaxies (e.g. Veilleux et al. (1995)), with the classical Balmer lines ($\text{H}\alpha$ and $\text{H}\beta$ essentially) and forbidden lines of oxygen (3727, 5007, and, less often, 6300Å), nitrogen (6548, 6584Å) and sulfur (6717, 6731Å). In most cases, the excitation is low, and the continuum appears to be reddened, so that quite often the $\text{H}\beta$ or [OIII] lines are not even detected. Because the $\text{H}\beta$ emission, when detected, is often superposed on the corresponding absorption line, the correct estimate of its intensity would require a proper determination (and subtraction) of the underlying absorption, which was not possible with the available spectra. We therefore have not derived an estimate of the reddening from the $\text{H}\alpha/\text{H}\beta$ ratio. This prevents us from deriving reliable $\text{H}\alpha$ luminosities, even for those objects observed under photometric conditions: the values given are therefore only lower limits.

We have not detected any broad Balmer line objects in this sample. The signal to noise ratio in the continuum would however not have allowed us to detect faint, broad wings in most cases (for Seyfert types 1.9 or 1.8). But we have a number of objects where the [NII]/ $\text{H}\alpha$ ratio is larger than the usual HII region limit of 0.5 (e.g. Veilleux (2002)), and so is the [SII]/ $\text{H}\alpha$ ratio, therefore indicating the presence of an AGN. Only exceptionnaly are other line ratios available, preventing a more precise classification of this AGN: the usual weakness or absence of the [OIII] line however points preferentially towards a Liner rather than a Seyfert 2 galaxy. We have 8 such cases out of a total of 50 objects, that is 15 %, a proportion similar to the one found in other IR-selected samples of low redshift objects with moderate IR luminosities.

ID	Coordinates ^a	cz (km/s)	r' Mag.	Emission (H α flux)	Absorption	Comments
FN1-000	160552.8+540651	43604 \pm 87	17.94	H α (183), [NII], [OI], [NI], H β , [OIII] H γ , [OII], (HeI)	Na	Liner
FN1-001	160736.6+535730	9004 \pm 51	16.67	H α (93.9), [NII], [SII], H β , [OIII], HeI	Na, Ca, (Mg), G, H, K	
FN1-002	161005.8+541029	19119 \pm 119	17.73	H α (13.9), [NII], [SII], H β , [OII]	Na, Mg, G, H, K	
FN1-003	161254.1+545526	19481 \pm 90	17.13	H α (21.7), [NII], [SII], [OII]	Na, (H β , Mg, Ca, G, H, K)	Em. with small EW
FN1-004N	161109.5+535807	19107 \pm 85	16.84	H α (9.5), [NII], [SII], [OIII]	Na, H β , G, Mg	Sey2, [NII]/H α >1
FN1-004S	161107.2+535711	19208 \pm 88	19.03	H α (5.5), [NII], [SII]	Na, G	
FN1-005	160443.4+543331	86400 ^b	19.22			
FN1-006	160433.9+544432	22608 \pm 63	17.26	H α (34.8), [NII],[SII], [OII]	Na, Mg, H β , G, H δ , H, K	
FN1-007	161331.2+541630	18435 \pm 41	17.18	H α (59.1), [NII], [SII], [OII]	Na, G, H, K	
FN1-009	160803.7+545302	15746 \pm 865	16.58	H α (17.0), [NII], [SII] [OI], [OIII], [OII]	Na, Mg, Ca, H β , H γ , H δ G, H, K	Liner
FN1-011	160808.6+535242	19326 \pm 48	17.84	H α , [NII], [SII], H β	Na, Ca, G, (H), K	
FN1-012	161214.0+540833	19770 \pm 73	17.88	H α (32.7), [NII], [SII], H β , [OIII], [OII]	Na, Mg, Ca, H, K	
FN1-014	161551.4+541536	21000 ^c	19.20			
FN1-015	160724.7+541212	70183 \pm 58	18.89	H β , [OII]	H, K	
FN1-016	16-738.0+544602	27579 \pm 85	17.09	H α (48.7), [NII], [OII]	Na, (H β), (H γ), H δ , H, K	
FN1-018	161407.1+541920	25598 \pm 105	18.92	H α (7.9), [NII], ([OIII]), [OII]	Na	AGN ([NII]/H α ~1)
FN1-020	160812.3+545526	3000 ^c	19.72			
FN1-021	161308.0+545142	19349 \pm 39	18.18	H α , [NII], [SII], H β	Na	
FN1-021B	161319.2+545138	19983 \pm 18	18.04	H α , [NII], [SII], H β , [OIII]		

^a: J2000 position of the optical counterpart. ^b: Chapman (private communication) ^c: photometric estimate (Babbedge et al. (2004))

Table 4. Spectroscopic properties of the FIRBACK identified sources. The quoted uncertainty for velocities is the internal (1σ) error, and does not include the systematics (see text). Emission (or absorption) lines shown in brackets are seen, but not used for the velocity determination because of poor S/N. The H α flux is given, when conditions were photometric, in units of $10^{-16}\text{ergs}/\text{cm}^2/\text{s}$.

ID	Coordinates	cz (km/s)	r' Mag.	Emission ($H\alpha$ flux)	Absorption	Comments
FN1-023	160835.4+535020	18780 ± 26	18.94	$H\alpha(26.1)$, [NII], [SII], $H\beta$, [OIII], [OII]	Na	
FN1-024	160937.5+541259	25770 ± 60	18.36	$H\alpha(20.1)$, [NII], $H\beta$, ([OII])	Na	
FN1-026	161436.9+541635	23835 ± 12	19.10	$H\alpha(4.8)$, [NII]	(Na), ($H\delta$)	
FN1-031	161103.7+544322	18840 ± 78	17.69	$H\alpha(8.6)$, [NII], [SII], ([OIII])	H, K	
FN1-033	161301.1+541003	41173 ± 65	18.47	$H\beta$, [OII]	Na, G, H, (K)	
FN1-035	161527.7+543414	40820 ± 72	18.11	$H\alpha$, [NII], [OII]	Na, Mg, ($H\beta$), H, K	
FN1-038	160747.3+534836	32192 ± 20	19.26	$H\alpha(10.1)$, [NII], [SII], $H\beta$, [OIII]		
FN1-039	160848.9+545151	80700^b	20.18			
FN1-041	160814.2+542836	35995 ± 46	18.89	$H\alpha$, [NII], $H\beta$, [OIII], $H\gamma$		
FN1-043	160553.4+542226	63470 ± 53	18.69	$H\alpha$, [NII], [OII]	(G), H	

Table 4. Spectroscopic properties (continued)... For source FN1-040, $z = 0.45$, see Chapman et al. (2002)

ID	Coordinates ^a	cz (km/s)	r' Mag.	Emission (H α flux)	Absorption	Comments
FN1-008	160858.0+541818	78770 \pm 83	18.83	[OII]	Na, H, K	
FN1-010	160930.9+535148	18741 \pm 75	17.18	H α (9.1), [NII], [SII]	Na, Mg, Ca, H β , G, H, K	Prob. AGN (NII/H α >0.5)
FN1-019	161235.4+541545	18663 \pm 104	17.05	H α (5.0), [NII], [OI], [OII]	Na, (Mg), H β , G, H, K	AGN ([NII]/H α >0.5)
FN1-025N	160833.4+545510	15761 \pm 37	18.81	H α , [NII], [SII], H β , [OIII], ([OII])	H	
FN1-025S	160834.5+545421	32671 \pm 54		H α , [NII], H β , [OIII], [OII]		
FN1-028A	160738.2+534250	19816 \pm 154	17.59		Na, Mg, H β , G, H, K	
FN1-028B	160746.5+534151	19921 \pm 142	16.70	[OII]	Mg, Ca, (H β), G, H, K	
FN1-029	161117.5+541629	43100 \pm 70	18.67	H α (11.4), [NII]	Na, H, K	
FN1-032	161239.9+543657	18674 \pm 63	17.38	H α (8.9), [NII], [SII]	Na, Mg, (H β), G, H, K	AGN (NII/H α \sim 1)
FN1-034	(160724.2+544330)	27916 \pm 54	18.66	H α (27.5), [NII], H β , [OIII], [OII]	K	
FN1-037	161509.0+541837	85500 \pm 300	19.42	[OII], [NeV]	Mg, K	Id. uncertain
FN1-042	161038.9+543628	18844 \pm 68	17.24	[NII]	Na, H β , Ca, Mg, H, K	AGN ([NII]/H α >1)
FN1-044	160931.6+541827	24682 \pm 41	18.69	H α (7.2), [NII], [SII], [OIII]	(Na), (G)	
FN1-045	160853.9+544735	276400?	19.24	[OII] ??		Single emission line
FN1-046A	161249.4+540837	45290 \pm 16	18.01	([NeV]??)	Na, Mg, (G), H, K	Radio source
FN1-046B	161251.1+540801	18566 \pm 73	17.38	H α , [NII], [SII], [OII]	Na, G, H, K	
FN1-048	161059.1+542305	18688 \pm 22	19.37	H α (10.8), [NII], [SII], H β , [OIII]	Na	
FN1-049	160801.6+543642	38381 \pm 107	18.89	H β , [OIII], [OII]	(H), K	
FN1-057	160801.6+543643	27546 \pm 35	18.43	H α (15.1), [NII]	Na, Ca, (G), H, K	
FN1-101	160946.1+542127	19690 \pm 58	18.44	H α , [NII], [SII], H β , [OIII], [OII]	H, K	

^a: J2000 position of the optical counterpart.

Table 5. Spectroscopy of additional sources (sources with multiple or uncomplete identification; or sources outside the 4σ sample (FN1-057 and FN1-101)).

The H α flux is given in parenthesis, in units of $10^{-16} \text{ergs}/\text{cm}^2/\text{s}$, when conditions were photometric.

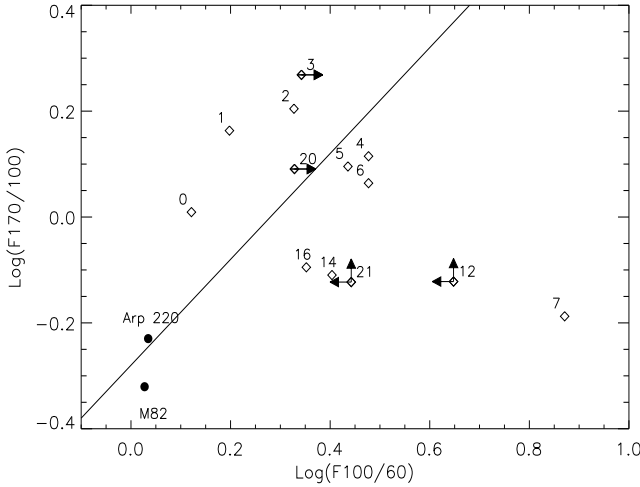


Fig. 3. 60, 100, 170 color ratios. The continuous line is the ISS fit, see text.

5. Mid and far-IR properties

5.1. For sources with IRAS detections: 60, 100 and 170 colors

The mean infrared (60, 100 and 170 μm) colors have been calculated for our identified galaxies. The two-color diagram $\log(F_{170\mu\text{m}}/F_{100\mu\text{m}})$ versus $\log(F_{100\mu\text{m}}/F_{60\mu\text{m}})$ (Fig. 3) includes all galaxies with measurements or upper limits in the 60 and 100 μm IRAS bands. The continuous line has a slope of ≈ 1 and corresponds to the least square bisector regression for the ISOPHOT 170 μm serendipity survey (ISS, Stickel et al. (2000)). Most of the galaxies have a behavior that is consistent with those from the ISS, apart FN1-007 (in the lower right corner of the figure; this object is peculiar, see the discussion of SEDs later on). Their colors are well within the sequence of the normal galaxy sample of Dale et al. (2001), and correspond more to the quiescent end of their classification (i.e. the coldest galaxies). Note that for Arp220 and M82, $\log(F_{100\mu\text{m}}/F_{60\mu\text{m}}) \approx 0.03$, and $\log(F_{170\mu\text{m}}/F_{100\mu\text{m}}) \approx 0.25$, ratios that are more typical of active galaxies.

5.2. The 15/170 μm color

Twenty four galaxies from our identified sample have both $F_{170\mu\text{m}}$ and $F_{15\mu\text{m}}$ measurements. We add to those sources FN1 – 013 and FN1 – 053 which do not yet have a redshift measurement but have a clearly identified 15 μm counterpart. From their $F_{170\mu\text{m}}/F_{15\mu\text{m}}$ ratio, the contribution of these 26 galaxies to the CIB can be estimated. The observed color of the CIB can be bracketted from the work of Elbaz et al. (2002) and Renault et al. (2001) : $30 < CIB_{170\mu\text{m}/15\mu\text{m}} < 75$. On the other hand, the model of Lagache et al. (2004), which reproduces (i) the number counts at 15, 24, 60, 70, 90, 160, 170 and 850 μm , (ii) the known redshift distributions (mainly at 15, 170

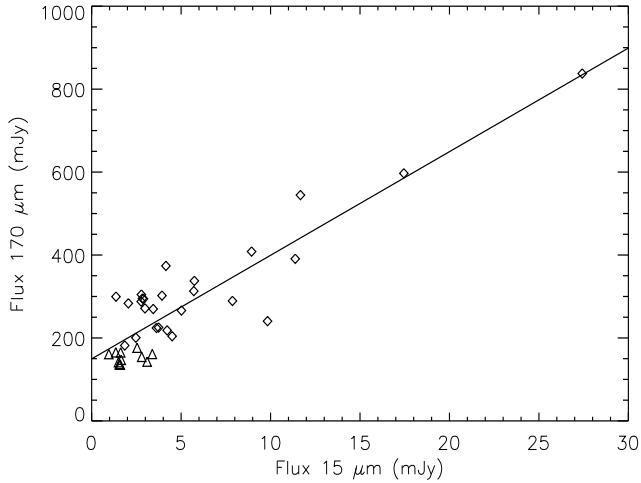


Fig. 4. 170/15 correlation. The diamonds are for $S_{170} > 4\sigma$ and the triangle for $3\sigma < S_{170} < 4\sigma$. The continuous line is the best fit for all sources. It has a slope of $170/15=25$.

and 850 μm), (iii) the local luminosity functions at 60 and 850 μm and (iv) the CIB (from 100 to 1000 μm) and its fluctuations (at 60, 100 and 170 μm), gives a ratio $CIB_{170\mu\text{m}/15\mu\text{m}} = 59.4$. In view of the excellent agreement of the Lagache et al. (2004) model with the observations from the mid-IR to the mm range, and the fact that the CIB color from the model lies well within the range given by the observations, we take this value from the model (60) as the best estimate of the 170/15 color of the CIB.

The 170/15 relation for the observed FIRBACK galaxies is shown in Fig 4. For sources with $S_{170} > 4\sigma$, the slope of the correlation is equal to 22.3. If we add to this sample the sources with $3\sigma < S_{170} < 4\sigma$, which are not identified optically, but have clear 15 μm counterparts, the slope increases from 22.3 to 25, but is still more than a factor of 2 below the mean color of the CIB as discussed above. These sources are thus clearly not representative of the bulk of the sources contributing to the 170 μm CIB. This is not surprising, as (1) it was shown by Dole et al. 2001 that the bright FIRBACK sources (down to the 3σ limit of the survey) represent in practice less than 5% of the CIB at 170 μm and (2) the observed CIB 170 $\mu\text{m}/15 \mu\text{m}$ ratio is about three times higher than that of the galaxies studied here, and is better matched with higher z sources due to the K-correction (around $z \sim 0.8$, as observed by Elbaz et al. (2002)).

5.3. Spectral Energy Distributions

5.3.1. Comparison with template spectra

To derive an IR luminosity when only a few sampling points are available, the most reliable technique is to identify a template spectrum whose Spectral Energy Distribution

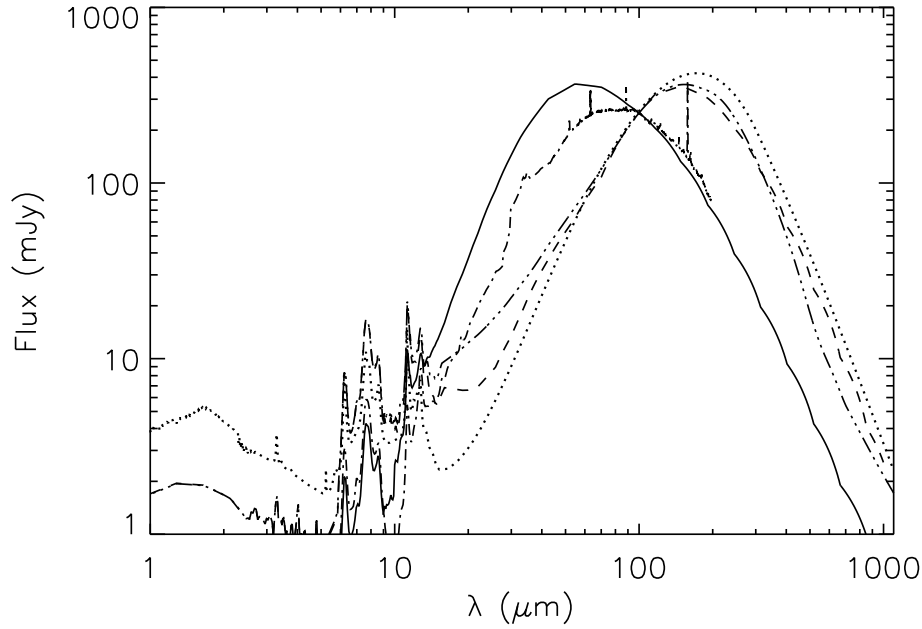


Fig. 5. Comparison of template SEDs from Dale et al. (2001) ($\alpha=2.6$, quiescent case, dashed line; and $\alpha=1$, active case, continuous line) and Lagache et al. (2003) (“cold galaxy”, triple-dot-long-dashed line) with observed SED’s. The dotted line is the observed SED of M101, the dashed-dotted line the SED of M82 (curves normalised at 100 μm).

(SED) best matches the observations (although the solution might not be unique). There are plenty of SEDs that could be tried: the ones we used are shown in Fig. 5 and are discussed below. Our first tests have shown (see also Patris et al. (2003)) that typical starbursts SEDs like (M82) did not match the data, and that colder components were required. We thus used template spectra from Lagache et al. (2003), most notably their “normal-galaxy” spectrum, that is derived from observations of a sample of galaxies with measurements from 15 to 850 μm (it was built essentially from cold galaxies, including those from the present sample, and will therefore be called “the cold template” in what follows, to avoid confusion). This “cold-galaxy” template has been fitted to each of our objects, and is shown as a solid line superposed on the observed points in Fig. 6 and Fig. 7. The SED of the typical starburst galaxy M82 is also shown as a dashed line. The important point to note is that the M82 template, although fitting quite well the 170/15 color, fails to reproduce the spectra at 60 and 100 μm . This template, although widely used, is not appropriate for the FIRBACK sources, which are colder galaxies.

For a quantitative appraisal of the contribution of various components, we use the models of Dale et al. (2001, 2002): they have modeled the infrared spectral energy distribution of normal star-forming galaxies, as a function of a parameter α which quantifies the relative contribution of “active” and quiescent regions from galaxy to

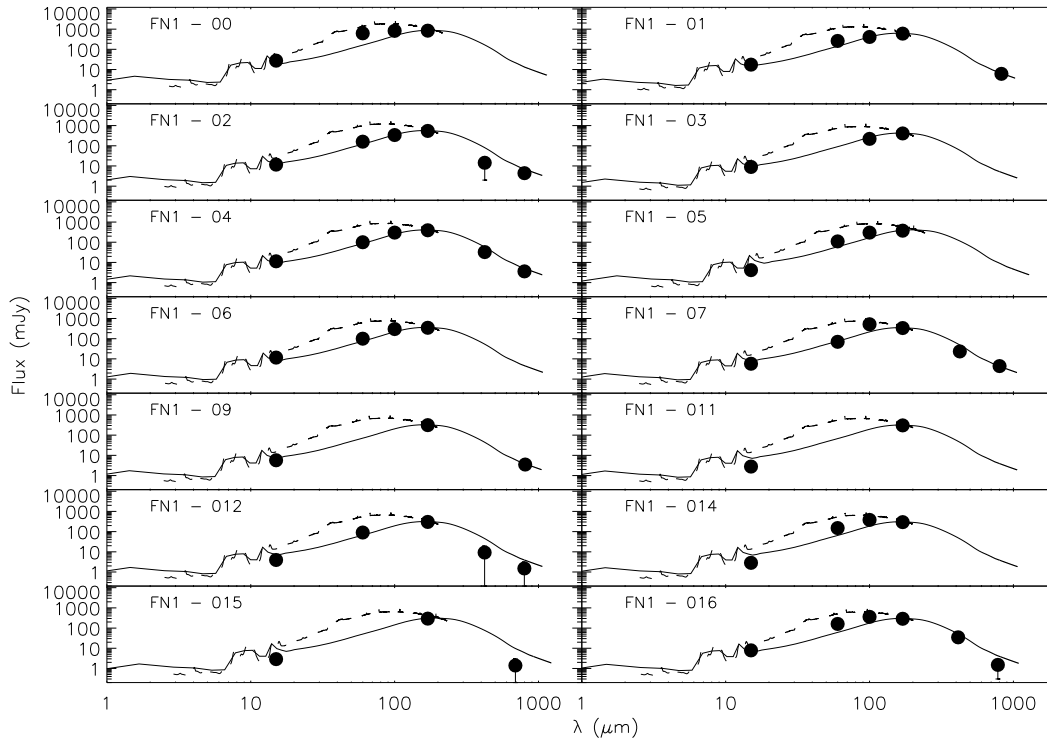


Fig. 6. The results from the fit of the source SEDs with a “cold galaxy” spectrum from Lagache et al. (2003). The continuous line is the “cold galaxy” spectrum template, the dashed line the spectrum of M82.

galaxy, $\alpha \approx 2.6$ being at the quiescent end and $\alpha \approx 1$ at the active end. Nine of our identified galaxies have both $F_{60\mu\text{m}}$ and $F_{100\mu\text{m}}$ measurements available and all but *FN1 - 007* have a $(F_{60\mu\text{m}}/F_{100\mu\text{m}})$ ratio that falls in the range of colors modeled by Dale et al. (2001, 2002). From the observed $(F_{60\mu\text{m}}/F_{100\mu\text{m}})$ ratio, we derive α , and the corresponding best fit template spectrum. The best fit template spectra from Dale et al. (2002) are shown in Fig. 8. The derived α (Table 6) corresponds always to models where the quiescent component dominates ($\alpha > 1.6$): this clearly shows that our sample is composed of preferentially cold galaxies with only moderate star formation, rather than more active objects where the $F_{60\mu\text{m}}/F_{100\mu\text{m}}$ is usually greater than 1.

The chi squared of the two fits (the Dale et al. set or the Lagache et al. “cold galaxy” spectrum; the M82 template is clearly not adequate, as can be seen from the figures) have been compared. The Dale et al. template spectrum is a better fit for only *FN-000* and *FN-016*, while it is comparable to the “cold galaxy” spectrum fit for the other galaxies. The *FN-007* object remains an exception, but its optical spectrum does not give any indication of a peculiar nature. Its SED is however peculiar, with a very high $F_{100\mu\text{m}}/F_{60\mu\text{m}}$ and a comparatively low $F_{170\mu\text{m}}/F_{100\mu\text{m}}$ ratio, difficult to explain with

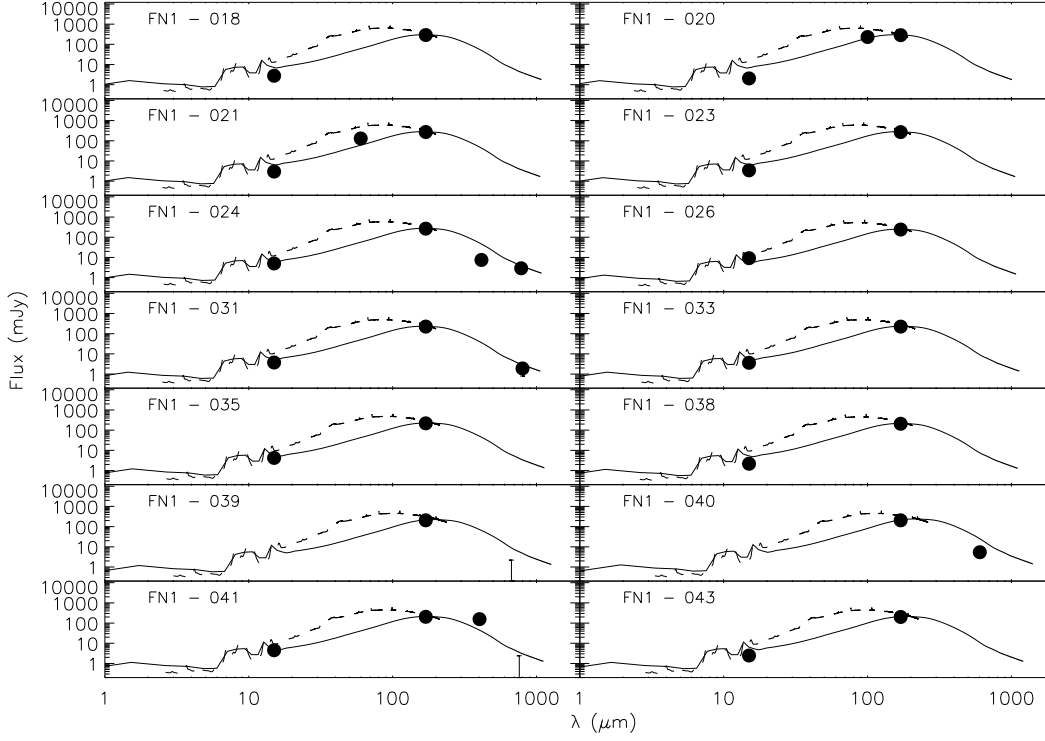


Fig. 7. Same as in Fig 6 for the remaining identified sources.

standard components. On average, the FIRBACK sources are clearly cold galaxies.

5.3.2. IR luminosities

Total luminosities have then been calculated in several ways. First by integrating the best fit spectra between 1 and 1000 μm . This was done for all sources with the "cold" spectrum, even for those where only one measured point was available, namely the 170 μm flux. The derived values are shown in Table 6. For those objects where a "Dale" spectrum could be determined, the luminosity is also derived (Table 6). Note that this second method was not applied to FN1-007, although it has measured 60 μm and 100 μm fluxes, because its color lies outside the range of validity of Dale's models. Finally, we used also the formula proposed by Stickel et al. (2000) to calculate luminosities when fluxes at 60, 100 and 170 μm were available. Following their formula :

$$F_{40-220} = 1.34 \times 10^{-14} \times (2.58F_{60\mu\text{m}} + 1.00F_{100\mu\text{m}} + 0.63F_{170\mu\text{m}}) \text{ Wm}^{-2} \quad (1)$$

$$F_{1-1000} = 1.35F_{40-220} \text{ Wm}^{-2} \quad (2)$$

$$L_{1-1000} = 4\pi D^2 F_{1-1000} \quad (3)$$

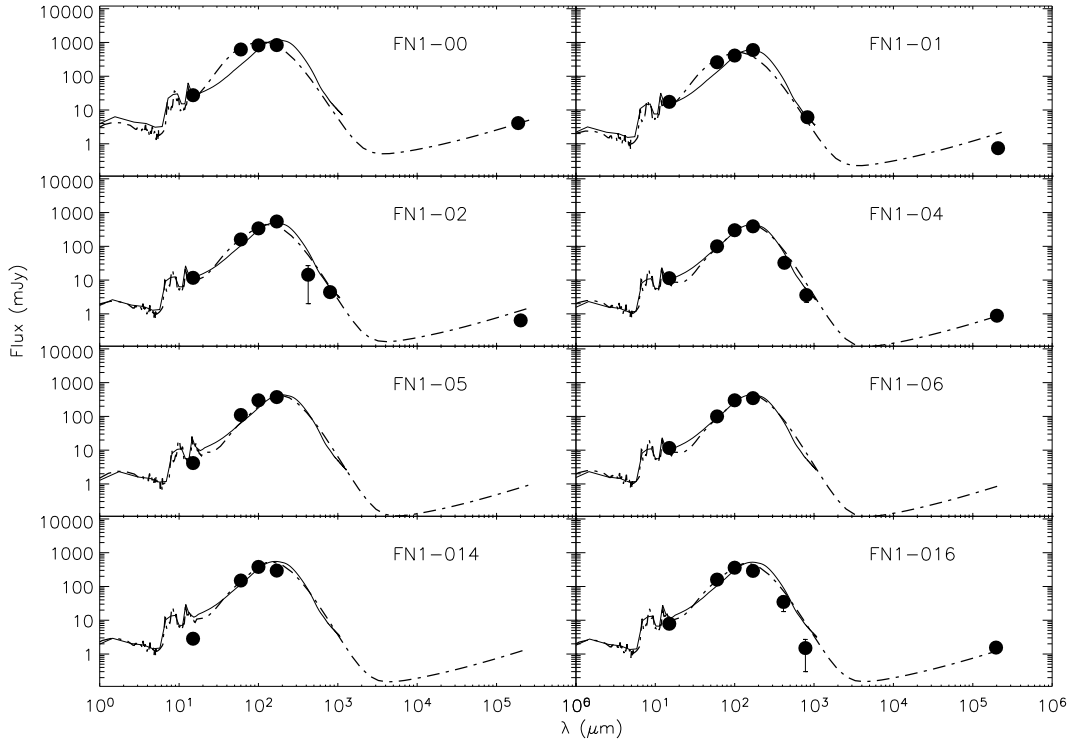


Fig. 8. SEDs of those identified sources that have both measured 60 μm and 100 μm fluxes are fitted with a Dale model. The dashed-dotted line is the Dale model fit, the thin continuous one the “cold galaxy” spectrum template (Lagache et al. (2003)). Both the model and the template have been normalized at 170 μm .

where D is the luminosity distance. The luminosities derived with this formula are also shown in Table 6.

For sources for which 60 and 100 μm fluxes are available, the estimated luminosities can be compared. The luminosities estimated from Dale’s best fit model are generally higher than the luminosities derived by the two other methods: this can be attributed to the fact that Dale’s models better take into account the contribution from the cold emission at very long wavelengths. But the differences are always smaller than a factor of two, and generally lower than 30 %. In the subsequent analysis, we shall use (unless otherwise stated) the luminosity calculated from the Lagache model, as it is available for all objects.

6. The radio-FIR relation

The far-IR (FIR)-radio relation was introduced by Helou et al. (1985) from the study of normal galaxies with IRAS, and was shown to be quite general for various samples of galaxies (see Condon (1992) for a review). The tightness of the relation, and its small

ID	z	Lagache Lum. ($10^{10} L_{\odot}$)	Stickel L. ($10^{10} L_{\odot}$)	Dale L. (and α) ($10^{10} L_{\odot}$)	H α L. ($10^6 L_{\odot}$)	K Lum. ($10^9 L_{\odot}$)	SFR(IR) M_{\odot}/yr	SFR(H α) $10^{-2} M_{\odot}/\text{yr}$	q
0	0.145	52.3	73.0	95.3 (1.69)	222	5.87	68	>675	2.30
1	0.030	1.5	1.3	1.8 (1.83)	4.9	0.70	1.9	>15	2.69
2	0.063	6.4	4.6	6.1 (2.07)	3.2	2.32	8.3	>9.7	2.60
3	0.063	4.9			5.2	2.54	6.4	>16	
4	0.063	4.6	3.4	5.2 (2.52)	2.2	4.97	6.0	>6.7	2.32
5	0.288	100.8	70.5	113.6 (2.35)			131		
6	0.073	5.6	4.4	7.2 (2.52)	11.3	2.80	7.3	>34	
7	0.063	3.6	3.8		12.8	2.14	4.7	>39	2.35
9	0.053	2.4			2.8	3.14	3.1	>8.5	
11	0.063	3.6			3.0	1.39	4.7	>9.1	
12	0.063	3.8			8.2	0.93	4.9	>25	2.66
14	0.07	4.1	4.8	7.9 (2.25)			5.3		
15	0.23	48.6				4.23	63		
16	0.090	6.8	8.5	13.3 (2.13)	23.6	3.02	8.8	>72	2.22
18	0.067	6.0			3.3	2.22	7.8	>10	
20	0.01	0.1					0.13		
21	0.064	3.2			3.6	1.61	4.1	>11	
23	0.063	3.1			5.9	0.89	4.0	>18	
24	0.086	5.7			8.5	1.89	7.4	>26	
26	0.077	4.3			1.7	1.28	5.6	>5.2	
31	0.063	2.6			1.9	1.15	3.4	>5.8	
33	0.133	12.4					16.1		
35	0.137	11.9			32.5	5.30	15.5	>99	
38	0.107	6.9			6.7		9.0	>20	
39	0.269	47.6				2.23	62		
40 ^a	0.45	122.9				0.17	160	2000	
41	0.12	8.6				1.22	11.1		
43	0.21	27.5			21.1	7.23	36	>64	
49	0.127	9.8				3.39	12.7		

^a: Data from Chapman et al. 2002, main component, reddening corrected H β luminosity.

Table 6. Source luminosities calculated from the integrated “normal-galaxy” spectrum (Lagache Lum.), Stickel’s formula (Stickel Lum.) and the best fit Dale spectrum (Dale Lum.) with its α value. The H α luminosities, uncorrected for extinction (hence the “>” sign in the corresponding SFR), are also given. The K luminosity is directly derived from the K magnitude. The “q” parameter is the logarithmic ratio of IR to radio flux, following Helou et al. (1985).

dispersion, is best represented by the "q" parameter introduced by Helou et al. (1985), which is the ratio of FIR (as measured by IRAS) to the radio continuum (1.4 GHz) flux densities:

$$q = \log[(FIR/3.75 \times 10^{12} \text{ Wm}^{-2})/(S_\nu/\text{Wm}^{-2}\text{Hz}^{-1})] \quad (4)$$

where FIR is the 40-120 μm flux density derived from IRAS measurements via:

$$FIR/\text{Wm}^{-2} = 1.26 \times (2.58S_{60\mu\text{m}} + S_{100\mu\text{m}}) \quad (5)$$

The average value for q was found to be around 2.3 with a scatter lower than 0.2 (Helou et al. (1985)).

We can calculate this parameter for those FIRBACK objects where IRAS data are available, and found similar values (Table 6): the objects lie slightly above the mean relation, with an average of 2.45 for 8 objects. To increase the number of objects, one could calculate backwards a FIR from the integrated IR luminosity (for instance from the "Lagache" luminosity which is available for all of them, see previous section): this would then represent a FIR_{1-1000} instead of FIR_{40-120} and, as expected, the q ratio is increased accordingly. But only few objects are added this way (due to the limited radio detections), so that no advantage is obtained in practice from this different approach.

The main result is that no object has a q value significantly lower than the average 2.3 found in normal galaxies: there is therefore no evidence for a significant contribution to the total energy balance from a radio-loud AGN in any of those objects. For those few objects where the presence of an AGN is indicated from the spectroscopic data, and where radio data are also available, the q ratio is not higher, suggesting that the contribution of the AGN to the FIR flux is also negligible. However, we cannot exclude a contribution from a radio-quiet AGN.

7. Star formation rates

Several indicators can be used to estimate the Star Formation Rate (SFR) of galaxies, but it is widely accepted that the far-IR luminosity gives the best estimate, because it measures the bolometric luminosity of the object: this is correct as long as one can be sure that a hidden AGN is not significantly contributing to the total energy output. We have used the IR luminosity computed from the fit of the "Lagache" template (which is available for all the identified objects) and derived the SFR with the calibration of Devriendt et al. (1999):

$$\text{SFR} (M_\odot \text{ per year}) = \frac{L_{\text{IR}} (10^9 L_\odot)}{7.7}$$

The result is given in Table 6. Most of the objects have star formation rates of only a few M_\odot/year and are therefore moderate starbursters only. Five objects are

however standing out: $FN1 - 000$, $FN1 - 005$, $FN1 - 015$, $FN1 - 039$, and $FN1 - 040$. $FN1 - 005$ and $FN1 - 040$ are the most distant objects in this limited sample of fully identified sources, and are clearly ULIRG's detected at larger distance than the average, bright, FIRBACK sources (for details on $FN1 - 040$, see Chapman et al. 2002). The same is true for $FN1 - 015$ although it has a three times smaller IR luminosity. For $FN1 - 039$ we have no detailed information. More interesting is the case of $FN1 - 000$, which is closer, and at similar distances than, for instance, $FN1 - 035$ or $FN1 - 033$, but has a five times greater luminosity. We have no evidence that an AGN is located inside this galaxy neither from spectroscopy nor from the q parameter, so we consider it as a vigorous, local starburst galaxy.

We can, in principle, also use the $H\alpha$ luminosity to derive the SFR, following the recipe of, e.g., Kennicutt (1992):

$$\text{SFR (M}_{\odot}\text{ per year)} = \frac{L_{H\alpha} (10^{41}\text{erg/s})}{1.26}$$

The result is also given in Table 6. For the 17 objects where we have both IR and $H\alpha$ estimates, the latter always gives a much lower SFR, on average a factor of 22 lower than the former one (note that the 4 high-luminosity objects are not included in this sample). This is clearly due to the fact that our $H\alpha$ fluxes are not corrected for internal extinction. We have no reddening estimate for each individual galaxy. In a few cases only, like $FN1 - 000$, an extinction can be estimated from the $H\alpha$ over $H\beta$ ratio (where we find $A_v = 2$, with the necessary caveat due to the unresolved underlying absorption lines). We could apply to the whole sample an average extinction correction of $A_v \sim 1$, as was done in other cases (e.g. Pettini et al. (2001) where a low extinction was estimated from the comparison between UV and visible properties or Lilly et al. (2003) where this value was derived from a local reference sample). It is however very unlikely that such a low extinction would be appropriate for our sample which is mainly emitting in the far IR. Instead, we can use a value obtained from a very similar sample where more data are available, namely the FIRBACK southern field (Patris et al. (2003)): the average extinction found there is $A_v = 3$. This corresponds to an upwards correction of a factor of 10 to the SFR derived from the $H\alpha$ luminosities. While such a correction is only indicative, because the dispersion of extinction values from object to object may be very high, the similarity of these two samples ensures that the selection effects are minimized: this value is certainly more appropriate than the standard $A_v = 1$ value applied in other samples. After such correction, it appears that the SFR derived from $H\alpha$ becomes closer to the one derived from the IR, although still systematically lower. The remaining difference is due in part to some slit losses and, more probably, to a large optical thickness in $H\alpha$ that prevents an accurate extinction correction. This problem is

similar to the one encountered in other IR selected samples (like in Patris et al. (2003)) but without additional data, the comparison between the various SFR estimators cannot be pursued further.

The radio-FIR relation, discussed in the previous section, shows however that the "q" parameter for these galaxies (at least the 8 for which it could be determined) is not significantly different from the standard value found by Condon & Broderick (1991) in the Bright Galaxy Sample of Soifer et al. (1989): 2.4 for our objects instead of 2.3 in the BGS. Our galaxies, with the exception of the 5 cases mentioned above, are thus effectively moderate starbursters only.

8. Discussion and conclusions

Out of the 56 FIRBACK N1 sources with 170 μm fluxes above the 4σ limit of 180 mJy, 28 have been firmly identified and 17 others have at least one of the contributors identified. Only 11 sources remain unclear, essentially due to the lack of additional data (radio or near-IR) with better positional accuracy. Most of the identified sources are quiescent star-forming galaxies which exhibit a colder spectrum than a standard IRAS starburst galaxy. There is no overlap with the catalogue of galaxies resulting from the ISOPHOT 170 μm Serendipity Survey (Stickel et al. 2004), although in view of their detection limit of $\sim 0.5Jy$ one would have expected that the first 3 objects from the FIRBACK-N1 catalogue could have been found there. We can nevertheless compare the properties of our objects that have also detected IRAS fluxes with those from the Serendipity Survey discussed by Stickel et al. (2000). Both samples have similar far-IR colours, with an $F_{100\mu\text{m}}/F_{60\mu\text{m}}$ ratio greater than ~ 1.5 and a $F_{170\mu\text{m}}/F_{100\mu\text{m}}$ greater than 0.7, which we qualify as "cold" galaxies, dominated by a cold dust component with temperatures roughly between 20 and 40K. This is clearly different from the "warm" LIRGs and ULIRGs, whose $F_{100\mu\text{m}}/F_{60\mu\text{m}}$ ratio is generally close to or smaller than 1, and which are strong starbursters. The bright FIRBACK galaxies seem therefore to represent a fainter version of the "cold" galaxies detected in the Serendipity Survey.

In terms of optical spectral properties, they resemble the faint IRAS galaxies selected by Bertin et al. (1997) and described in Patris et al. (2003): emission lines, moderate to strong reddening and moderate SFR. There is unfortunately no IR colour information available for the Bertin et al. (1997) sample, for comparison, as those galaxies represent the faintest objects detected in the IRAS survey, in the most sensitive channel ($F_{60\mu\text{m}}$ between 150 and 250 mJy), and are thus not detected in the other channels. It seems however clear, from the three different samples just discussed, that a large population of "cold" galaxies exists at least in the local universe (with a few tens of objects per square degree), with moderate star formation, whose contribution to the global star formation rate is probably significant, although it has been rather neglected until now,

in the "rush" to find always more extreme starburst objects.

The bright FIRBACK galaxies studied here are mostly nearby, Luminous IR Galaxies (LIRGs) with moderate star-formation rates (about 5 to 10 M_{\odot}/yr) and are not particularly associated with detectable merging or interacting systems (only three mergers are clearly detected among the 28 fully identified objects). One could question whether they should be called "starbursts galaxies" or whether they do not simply represent disk galaxies with more quiescent star formation (or disks ionised by diffuse radiation). Recent Spitzer observations of classical spiral galaxies like the Scd spiral NGC 300 (Helou et al. 2004) or the Sc M33 (Hinz et al. 2004) show that their integrated SFR is low, of the order of 0.1-0.2 M_{\odot}/yr , and that, although their 160 μm emission might be more diffuse, the shorter wavelength emission is clearly associated with ionising stars. Such SFR are much smaller than the ones obtained for our FIRBACK galaxies. A larger sample of galaxies has been observed in $H\alpha$ by James et al. (2004) to derive SFRs: they find an integrated, extinction-corrected SFR of 1-3 M_{\odot}/yr for the most active spirals, the types Sbc or Scs. Our $H\alpha$ rates are difficult to compare directly because of the uncertain extinction correction: but either applying the average correction of 10 discussed earlier, or using individually corrected $H\alpha$ rates from the similar, southern sample discussed by Patris et al. (2003), or using the FIR-SFR which correlate well with the corrected $H\alpha$ rates as shown by Patris et al. (2003), we have here SFRs on average 3 to 4 times greater than the most active galaxies of James et al. (2004), the Scs. Furthermore, our morphologies are generally of earlier types than Sc (with often a central, bulky component), types for which the SFRs measured in James et al. (2004) are comparatively smaller. By comparison, M101, a nearly face-on spiral whose SED, shown in Fig. 5, is comparable to the quiescent one of Dale et al. (2001), has a FIR-SFR of 5.7 M_{\odot}/yr (for an IR luminosity of $4.4 \cdot 10^{10} L_{\odot}$, derived from IRAS data), similar to the ones of our FIRBACK galaxies. But its classification is SBc, again of later type than most of our galaxies, and furthermore with a bar, usually believed to be linked with larger SFRs than in non-barred galaxies.

The IR luminosity function derived from the Bright Galaxy Sample by Soifer et al. (1987) shows that the break occurs at a luminosity of $1.7 \cdot 10^{10} L_{\odot}$. Following Stickel et al. (2000), this value, calculated over the 40-220 μm range, converts into roughly $3 \cdot 10^{10} L_{\odot}$ for the 3-1000 μm range discussed in this paper: the majority of our objects are therefore typical L^* objects, or slightly above. Noticable exceptions are FN1-0, 5, 15, 39, 40 or 43, which are much more luminous. When comparing with the local K-band luminosity function of Cole et al. (2001), most of our galaxies are only slightly brighter than the M_K^* magnitude of -24.2 (with $H_0 = 70 \text{ km/s/Mpc}$ as used here) (the exceptions being FN1-1, 12, 23 and 40 which are significantly fainter), so that they are not extremely massive galaxies. The ratio of total far-IR luminosity to the K-band luminosity, which can be interpreted as an indicator of the ratio of present to past star

formation, is rather homogeneous for the sample, with values between 20 and 40, showing that the present SF dominates the energy output. A few objects are more active than average (FN1-1, 23, 39, 40, 41), but are also less massive (with the exception of FN1-39). The outstanding object is FN1-40 (which is also the most distant object of the sample), appearing as a sub-L* object from its K magnitude, but heavily forming stars, and with a far-IR luminosity bringing it into the ULIRG class: this galaxy is therefore clearly of a different nature than the average bright FIRBACK galaxy and is probably a dwarf galaxy experiencing one of its first starbursts; see also Chapman et al. 2002. We conclude that, while a few are standard, disk-dominated spirals (like for instance FN1-02), many of these objects seem to have a larger SFR than standard spirals, with a concentration towards the central regions which could indicate the final phase of a former merger event.

As far as the CIB is concerned, it is clear that the bright FIRBACK galaxies have mid- to far-IR colors clearly different from the mean colors of the CIB. They do therefore not represent the bulk of the sources contributing to the mid- and far-IR CIB, contrary to earlier expectations (e.g. Puget et al. (1999), or Devriendt & Guiderdoni (2000)). The main contributors to the IR-CIB are thus expected to be more distant, more active galaxies, which will possibly be detected within the fainter part of the FIRBACK survey.

This local cold population however has to be taken into account in the modelling of the evolution of IR galaxies. In practice, it strongly affects the redshift distribution of 170 μm sources predicted by the models. When models consider only starburst galaxies, they lead to a redshift distribution for the 4σ FIRBACK galaxies that is clearly biased towards redshifts much higher than those observed here (e.g. Devriendt & Guiderdoni (2000)). Our present results show that the number counts are dominated by local cold galaxies for 170 μm fluxes greater than about 240 mJy. This is now well taken into account in the Lagache et al. (2003) models, which predict an equal contribution of starburst- and of "cold" galaxies at 250 mJy. This is also in agreement with the statistical results derived from sub-mm observations by Sajina et al. (2003).

The detailed analysis of the FIRBACK population obviously needs to be completed by the identification of the fainter, more distant counterparts. This will require many complementary observations in various wavelength ranges, from the ground with larger facilities, and from space. But, as the confusion limit of the FIRBACK survey clearly restricts the detection to relatively nearby objects, results from *SPITZER* should notably improve the situation. Indeed, the first number counts at 24 μm in the N1 field by e.g. Chary et al. (2004) suggest a strong contribution from luminous IR galaxies in the redshift range between 0.5 and 2.5. Inclusion of the shorter wavelengths data from IRAC will also allow to better determine the contribution of the quiet, diffuse component to the overall energy output in the nearby objects. A detailed study of those

galaxies (which is underway; e.g. Sajina et al., in preparation) is therefore likely to bring new light on the evolution of IR galaxies and their relation to the higher- z sources found in sub-mm observations.

Acknowledgements: We thank Jean-Loup Puget for enlightening discussions and support during this work; P. Chaniel for providing the M101 data in advance of publication; S.C. Chapman for providing us two redshifts (FN1-5, 39) and D. Dale for providing his SED models. S.M. acknowledges support from the ESA External Fellowship program, and advice from Marc Postman for the morphological classification of the galaxies.

This paper is based on observations made with ISO, an ESA project with instruments funded by ESA Member States and with the participation of ISAS and NASA.

This publication makes use of data products from the Two Micron All Sky Survey, which is a joint project of the University of Massachusetts and the Infrared Processing and Analysis Center/California Institute of Technology, funded by NASA and NSF. It also used data from the Lyon Extragalactic Database (LEDA).

References

- Babbedge T.S.R., Rowan-Robinson M., Gonzalez-Solares E. et al., 2004, MNRAS 354, 961
- Basilakos S., Georgantopoulos I., Pérez-Fournon I. et al., 2002, MNRAS 331, 417
- Becker R.H., White R.L. & Helfand D.J., 1995, ApJ 450, 559
- Bertin E., Dennefeld M. & Moshir M., 1997, A&A 323, 685
- Chaniel P. 2003, Ph. D. Thesis, University of Paris-7
- Chapman S. C., Smail I., Ivison R.J. et al., 2002, ApJ 573, 66
- Chary R., Casertano S., Dickinson M.E. et al., 2004, astro-ph 0406386
- Ciliegli P., McMahon R.G., Miley G. et al., 1999, MNRAS 302, 222
- Cole S., Norberg P., Baugh C.M. et al., 2001, MNRAS 326, 255
- Condon J.J., Cotton W.D., Greisen E.W. et al., 1998, AJ 115, 1693
- Condon J. J., 1992, Ann. Rev. Astron. Astrophys. 30, 575
- Condon J. J. & Broderick J. J., 1991, AJ 102, 1663
- Dale D., Helou G., Contursi A. et al. 2001, ApJ 549, 215
- Dale D., & Helou G., 2002, ApJ 576, 159
- Devriendt J., Guiderdoni B. & Sadat R. 1999, A&A 350, 381
- Devriendt J. & Guiderdoni B. 2000, A&A 363, 851
- Dole H., Gispert R., Lagache G. et al. (FIRBACK III), 2001, A&A 372, 364
- Elbaz D., Cesarsky C., Chaniel P. et al. 2002, A&A 384, 848
- Flores H., Hammer F., Désert F.-X. et al. 1999, A&A 343, 389
- Gonzalez-Solares E.A., Perez-Fournon I., Rowan-Robinson M. et al. 2005, MNRAS in press, astro-ph 0402406
- Hauser M.G., Dwek E., 2001, ARAA, 37, 249
- Helou G., Soifer B. T., & Rowan-Robinson M. 1985, ApJ 298 L7
- Helou G., Roussel H., Appleton P. et al., 2004, ApJ Supp. 154, 253

- Heraudeau Ph., Oliver S., del Burgo C. et al., 2004, MNRAS 354, 924
- Hinz J. L., Rieke G. H., Gordon K. D. et al., 2004, ApJ Supp. 154, 259
- James P. A., Shane N. S., Beckman J. E. et al., 2004, A&A 414, 23
- Kawara K., Sato Y., Matsuhara H. et al. 1998, A&A 336, L9
- Kennicutt R.C. 1992, ApJ 388, 310
- Kessler M. F., Steinz J. A., Anderegg M. E. et al. 1996, A&A 315, 27
- Kleinmann S. G., Lysaght M. G., Pughe W. L. et al. 1994, Ap&SS 217, 11
- Lagache G., Dole H. & Puget J.L., 2003, MNRAS 338, 555
- Lagache G., Dole H. & Puget J.L., et al., 2004, APJSS, in press
- Lilly S.J., Carollo C.M. & Stockton A.N., 2003, ApJ 597, 730
- Lonsdale C. J., Smith H. E., Rowan-Robinson M. et al. 2003, PASP 115,897
- McMahon R. G., Walton N. A., Irwin M. J. et al. 2001, New A.R., 45, 97
- Mann R.G., Oliver S., Carballo R. et al. 2002, MNRAS 332, 549
- Manners J.C., Serjeant S., Bottinelli S. et al. 2004, MNRAS 355, 97
- Oliver S., Rowan-Robinson M., Alexander D.M. et al. 2000, MNRAS 316, 749
- Patris J., Dennefeld D., Lagache G., Dole H., 2003, A&A 412, 349
- Pettini M., Shapley A.E., Steidel C.C. et al., 2001, ApJ 554, 981
- Postman M. et al., 2005, ApJ submitted
- Puget J.-L., Abergel A., Bernard J.-P. et al., 1996, A&A 308, 5
- Puget J.-L., Lagache G., Clements D.L. et al. 1999, A&A 345, 29
- Renault C., Barrau A., Lagache G. and Puget J.-L., 2001, A&A 371, 771
- Rowan-Robinson M., Lari C., Perez-Fournon I. et al., 2004, MNRAS 351, 1290
- Sajina A., Borys C., Chapman S. et al., 2003, MNRAS 343, 1365
- Scott D., Lagache G., Borys C. et al., 2000, A&A 357, L5
- Soifer B. T., Sanders D. B., Madore B. F. et al., 1987, ApJ 320, 238
- Soifer B. T., Boehmer L., Neugebauer G. & Sanders D. B., 1989, AJ 98, 766
- Stickel M., Lemke D., Klaas U. et al., 2000, A&A 359, 865
- Stickel M., Lemke D., Klaas U. et al., 2004, A&A 422, 39
- Strateva I., Ivezić Z., Knapp G.R. et al., 2001, AJ 122, 1861
- Surace J. A., Shupe D. L., Fang F. et al., 2004, <http://ssc.spitzer.caltech.edu/legacy/>
- Vaccari M., Lari C., Angeretti L. et al., 2005, MNRAS in press, astro-ph 0404315
- Veilleux S., Kim D.C., Sanders D.B. et al., 1995, ApJ 98, 171
- Veilleux S., 2002, IAU Coll. 184, R.F. Green, E.Y. Khachikian and D.B. Sanders, Edts, ASP Conf. Series 284, 111
- Werner M. W., Roellig T. L., Low F. J. et al., 2004, ApJ Supp. 154, 1

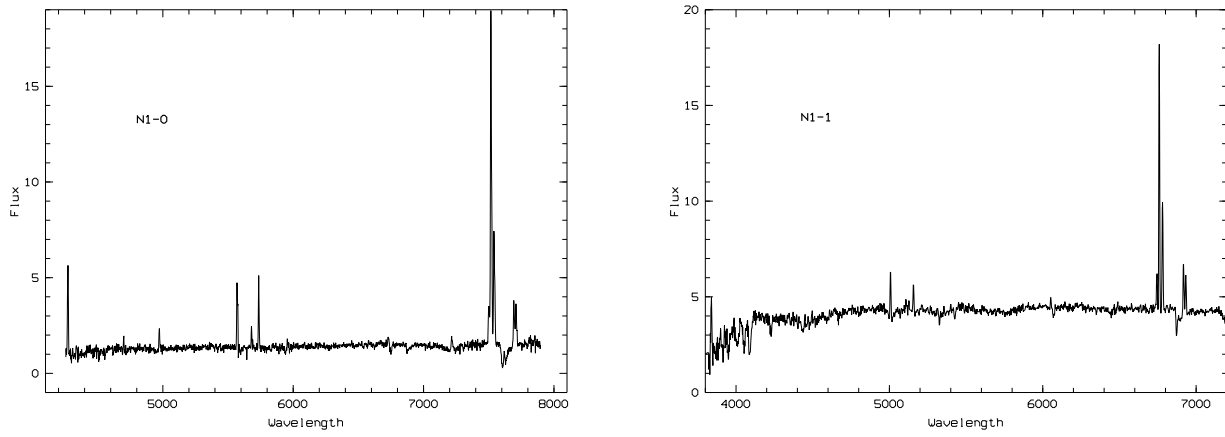


Fig. 9. Spectra of individual objects as examples (FN1-0 and FN1-1). Spectra of further objects are only available in electronic form.

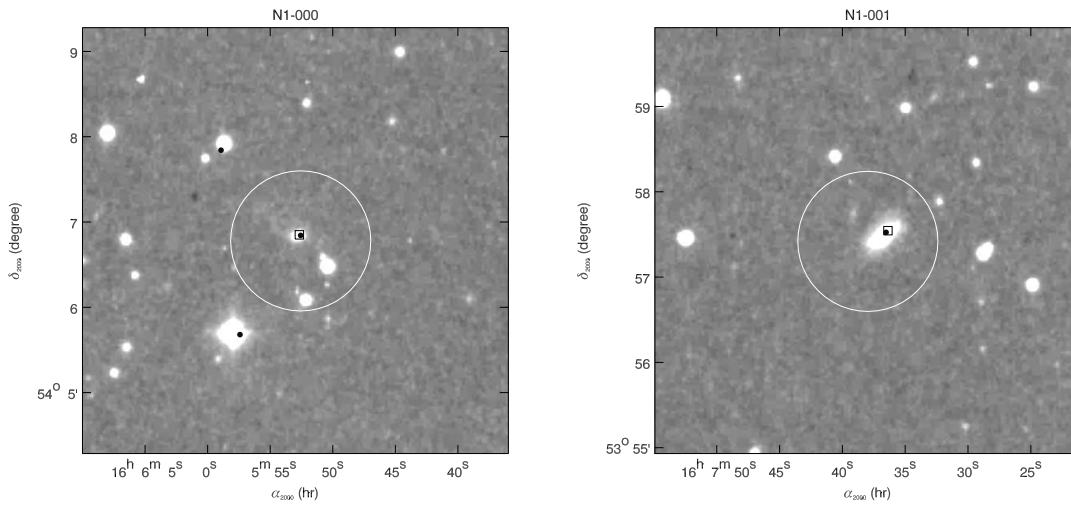


Fig. 10. Identification charts of FIRBACK N1 field sources (FN1-0 and FN1-1 as examples). Charts of further objects are only available in electronic form. The error circle for the 170 μm ISO source is superposed on the DSS optical image. An ISO 15 μm source is marked by a black dot and a radio source by a small open black square.